Department of Economics

Athens University of Economics and Business

WORKING PAPER no. 10-2026

Empirical Likelihood Tests for Pairwise Stochastic Dominance

Stelios Arvanitis, Richard McGee, and Thierry Post

July 2026

Πατησίων 76, 104 34 Αθήνα. Τηλ.: 210 8203303-5. E-mail: econ@aueb.gr / www.aueb.gr
76, Patission Street, Athens 104 34 Greece. Tel.: (+30) 210 8203303-5

The Working Papers in this series circulate mainly for early presentation and discussion, as well as for the information of the Academic Community and all interested in our current research activity.

The authors assume full responsibility for the accuracy of their paper as well as for the opinions expressed therein.

Πατησίων 76, 104 34 Αθήνα. Τηλ.: 210 8203303-5. E-mail: econ@aueb.gr / www.aueb.gr
76, Patission Street, Athens 104 34 Greece. Tel.: (+30) 210 8203303-5

Empirical Likelihood Tests for Pairwise Stochastic Dominance

Stelios Arvanitis[*], Richard McGee[†], and Thierry Post[‡]

July 8, 2026

Abstract

We develop an empirical likelihood test for pairwise stochastic dominance in weakly dependent time series. The procedure localizes candidate binding constraints as local minima of the empirical integrated distribution gap, then computes a multivariate empirical likelihood ratio over the resulting contact set. Critical values use re-centered pseudo-samples, implemented blockwise for dependence. The statistic is self-normalizing and covariance-adaptive, aggregating joint evidence from localized contacts rather than relying on a supremum or integrated support-wide distance. We prove first-order asymptotic validity and show that the null limit is a Gaussian-cone, or chi-bar-square, projection governed by the covariance of binding moments. Local-power results show equivalence between empirical likelihood and benchmark distance tests with one binding constraint, but possible power gains with multiple bindings because empirical likelihood exploits contact-set covariance geometry. Monte Carlo designs calibrated to option-enhanced indexation show accurate, stable size, robustness to the localization threshold, feasible calibration, and high power relative to Linton–Maasoumi–Whang and Linton–Song–Whang tests, especially when local violations align with covariance features captured by the statistic. An application to option-strategy indices rejects more economically implausible pairwise dominance relations, consistent with strategies trading off upside participation, option income, and downside protection rather than dominating each other.

[*]Athens University of Economics and Business, Greece. Email: stelios@aueb.gr

[†]University College Dublin, Ireland. Email: richard.mcgee@ucd.ie

[‡]Graduate School of Business of Nazarbayev University, Kazakhstan. E-mail: thierrypost@hotmail.com.
Funding from Nazarbayev University is acknowledged under the Faculty Development Competitive Research Grants Program (No. 201223FD8832) and Research Matching Grant Program (No. 110326MRP0303).

1 Introduction

Stochastic Dominance (SD) orders are widely used in Economics and Business because they provide robustness to misspecification of risk preferences and invariance to common data transformations; see, e.g., Levy (2016) and Perrakis (2019). Statistical testing is difficult because SD hypotheses involve a continuum of interdependent inequality restrictions on integrated CDF differences, creating partial-identification and boundary-inference problems.

Existing SD tests typically use Kolmogorov–Smirnov (KS), Cramér–von Mises (CvM), or empirical likelihood ratio (ELR) statistics, with critical values obtained from asymptotic approximations and resampling; see Whang (2019). In the present study, we develop the theory and implementation of an EL approach to pairwise SD testing for time-series data, using Linton et al. (2005) (LMW) and Linton et al. (2010) (LSW) as benchmarks.

Rather than measuring only the largest violation, as in KS statistics, or integrating squared violations over the support, as in CvM statistics, ELR asks how much the empirical distribution must be reweighted to satisfy the moment conditions. This approach evaluates the inequalities jointly and automatically normalizes for differences in variability and dependence across binding conditions. These features can help size control and improve test power when several nearly binding inequalities contain mutually reinforcing evidence. It builds on the general theory of EL and moment inequalities; see, e.g., Owen (1988), Kitamura (2006), Chen and Tabri (2019), Andrews and Soares (2010), and Andrews and Barwick (2012).

Despite this promise, the theory for EL-based SD tests remains incomplete. Existing applications have focused primarily on the null of pairwise non-dominance (Davidson and Duclos, 2013) and on multivariate generalizations such as stochastic optimality and stochastic efficiency (Post, 2017; Post and Potì, 2017). In many applications, however, the relevant null is dominance or a multivariate extension such as stochastic spanning (Arvanitis et al., 2019) and generalized stochastic arbitrage (Arvanitis and Post, 2023). For example, an active portfolio constructed in-sample under SD constraints is expected to dominate a benchmark out-of-sample if risk-arbitrage opportunities are present.

The distinction between non-dominance and dominance is material. Testing non-dominance is an interior problem because the null allows violations of dominance. Testing dominance is instead a boundary problem: the null is a closed system of inequalities, with nonstandard limiting behavior determined by the binding inequalities.

The main difficulty for EL dominance testing is the identification of the binding constraints and their joint sampling distribution. Slack inequalities are asymptotically irrelevant, but in finite samples they can appear nearly binding, inflate critical values, and reduce power. This problem is amplified in SD settings because the moment functions are nonlinear, nonsmooth transformations of the underlying data and nearby SD inequalities are strongly dependent.

We address this difficulty by exploiting the geometry of SD constraints. The SD inequalities are linked through the integrated distribution gap, whose derivative is the CDF difference. Informative interior contacts are generically isolated strict local minima of the gap function, while continuous contact sets require degenerate equality or flat-contact structures. We use this structure to localize candidate binding constraints as local minima of the empirical gap and compute the ELR on this localized set.

Critical values are obtained by applying a re-centered bootstrap to the localized constraints. The re-centering idea is shared with LMW, and the localization of candidate binding constraints is related to LSW, but here both are applied to a multivariate, self-normalized ELR, and localization is based on local minima, to reduce over-selection.

Our theoretical analysis establishes first-order exactness, conservativeness, and consistency under stationarity and absolute regularity. Under the null, the localized ELR converges to a Gaussian-cone, or chi-bar-square, limit determined by the covariance matrix of the binding moments. Under Pitman alternatives, local power differences arise from the multidimensional geometry of the binding space. With a single binding SD constraint, ELR, LMW, and LSW are locally equivalent; with multiple binding constraints and nonspherical covariance, ELR can achieve higher Pitman efficiency by aligning the rejection geometry with covariance-informative directions.

We examine finite-sample performance in Monte Carlo (MC) experiments calibrated to option-enhanced indexation, a standard financial application of SD. The design uses realistic stock index return parameters while allowing direct control over the number of binding constraints and the size and direction of local slackness or violations. The simulations show accurate and stable size for the proposed ELR test in the binding designs considered, robustness to the localization threshold, and high feasible power relative to the LMW and LSW benchmarks. The largest gains occur in multidimensional contact-set designs where violations align with covariance features captured by the ELR.

To illustrate the empirical and practical relevance of the choice of SD test, we apply the LMW, LSW, and ELR tests to a standard dataset of monthly returns on ten widely used Chicago Board Options Exchange (CBOE) S&P 500 index (SPX) option-strategy indices. Since these strategies trade off upside participation, option-premium income, and downside protection rather than being designed to dominate one another, pairwise dominance is unlikely a priori. The results show that ELR rejects substantially more economically implausible dominance relations than LMW and LSW, consistent with the power gains documented in the simulations.

For clarity, we focus on second-degree SD (SSD) between two choice alternatives. SSD is widely used because it has greater discriminatory power than FSD, corresponds to risk aversion, and is invariant under common transformations of the data. Extensions to higher-degree SD and to multivariate settings, including stochastic spanning, stochastic bounding, and stochastic arbitrage, are left for future research. For compactness, the proofs of the formal results and additional MC diagnostics are collected in the Online Supplement.

2 Preliminaries

2.1 Notation, objects and moment functions

Given an underlying probability space $(\Omega, \mathcal{F}, \mathbb{P})$, let Y be the reference random variable and X the comparison random variable. $\{(X_t, Y_t)\}_{t\in\mathbb{Z}}$ is a strictly stationary bivariate stochastic process on $(\Omega, \mathcal{F}, \mathbb{P})$ with marginal distributions F and G for X_t and Y_t, respectively. Throughout, we assume $\mathbb{E}[|X_t|] + \mathbb{E}[|Y_t|] < \infty$.

We use $\mathcal{Z} \subseteq \mathbb{R}$ for the convex hull of the union of the supports of F and G. $z_\star$ denotes the infimum of $\mathcal{Z}$, with the convention that it equals $-\infty$ when the set is not bounded below; this is generally not the case for investment returns. For $z \in \mathcal{Z}$, define the integrated CDFs (ICDFs), or lower partial moments, $F^{(2)}(z) := \mathbb{E}[\max(z - X_t, 0)]$ and $G^{(2)}(z) := \mathbb{E}[\max(z - Y_t, 0)]$. The finite-threshold component of SSD of X over Y, or $X \succeq_2 Y$, is defined using the ICDF gap function $\Delta(z) := G^{(2)}(z) - F^{(2)}(z)$ as $\Delta(z) \geq 0$ for all $z \in \mathcal{Z}$. The definition can equivalently be formulated in terms of the moment function $g_z(X_t, Y_t) := \max(z - Y_t, 0) - \max(z - X_t, 0)$, $z \in \mathcal{Z}$, because $\Delta(z) = \mathbb{E}[g_z(X_t, Y_t)]$.

If the mean inequality $\mathbb{E}[X_t - Y_t] \geq 0$ is imposed explicitly in the dominance relation, we include an index point at infinity and the associated moment function $g_\infty(X_t, Y_t) := X_t - Y_t$, with the convention that $\Delta(\infty) := \mathbb{E}[X_t - Y_t]$. This formalizes the boundary SD condition corresponding to the supremum of the support. In that case, we work with the augmented non-trivial index set $\mathcal{Z}_\infty := (\mathcal{Z} \setminus \{z_\star\}) \cup \{\infty\}$. If the mean restriction is not imposed, the point ∞ and all corresponding terms are omitted.

The null and alternative hypotheses of interest are

$$\mathbf{H}_0 : \ \Delta(z) \geq 0 \quad \forall z \in \mathcal{Z}_\infty; \ \mathbf{H}_1 : \ \exists z \in \mathcal{Z}_\infty \text{ such that } \Delta(z) < 0. \tag{1}$$

$\mathcal{Z}_T = \{z_{T,1} < \cdots < z_{T,m_T}\}$, $\mathcal{Z}_T \subset \mathcal{Z}$, denotes the (possibly random) set of threshold points actually used at sample size T. It is assumed to approximate sufficiently well the finite part of the limit set, in the sense that $m_T \to \infty$ as $T \to \infty$ and the mesh size of $\mathcal{Z}_T$ converges to zero, with neighborhoods of any finite contact points contained in $\mathcal{Z}_T$ with probability approaching one. When the mean restriction is imposed, the implemented constraint set is $\mathcal{Z}_{T,\infty} := \mathcal{Z}_T \cup \{\infty\}$; otherwise $\mathcal{Z}_{T,\infty} := \mathcal{Z}_T$.

The following empirical counterparts will be used:

$$\Delta_T(z) := \frac{1}{T}\sum_{t=1}^{T} g_z(X_t, Y_t);\ \mathbb{G}_T(z) := \sqrt{T}\{\Delta_T(z) - \Delta(z)\}. \tag{2}$$

For $z = \infty$, this definition gives $\Delta_T(\infty) := T^{-1}\sum_{t=1}^{T}(X_t - Y_t)$. The process $\{\mathbb{G}_T(z)\}_{z\in\mathcal{Z}_\infty}$ is viewed as an element of $\ell^\infty(\mathcal{Z}_\infty)$, i.e., the space of bounded real functions on $\mathcal{Z}_\infty$.

The population contact set consists of the non-trivial binding SD constraints: $C := \{z \in \mathcal{Z}_\infty : \Delta(z) = 0\}$. Equivalently, $C = C_f \cup C_\infty$, where $C_f := \{z \in \mathcal{Z} \setminus \{z_\star\} : \Delta(z) = 0\}$, and $C_\infty = \{\infty\}$ if the mean restriction is imposed and $\Delta(\infty) = 0$, with $C_\infty = \emptyset$ otherwise.

Although $\Delta(z_\star) = 0$, $z_\star$ is considered a trivial contact point in the sense that the corresponding moment inequality is non-informative about the validity of the dominance relation. The number of non-trivial contact points, $J := |C|$, is assumed to be finite; this assumption is motivated in the next subsection.

Given $C = \{z_1, \ldots, z_J\}$, define the binding moment vector

$$\mathbf{g}_C(X_t, Y_t) := \big(g_{z_1}(X_t, Y_t), \ldots, g_{z_J}(X_t, Y_t)\big)^\top, \qquad \bar{\mathbf{g}}_{C,T} := \frac{1}{T}\sum_{t=1}^{T}\mathbf{g}_C(X_t, Y_t). \tag{3}$$

If $z_j = \infty$, the corresponding component of $\mathbf{g}_C(X_t, Y_t)$ is $g_\infty(X_t, Y_t) = X_t - Y_t$.

Let Σ denote the long-run covariance matrix of $\sqrt{T}\bar{\mathbf{g}}_{C,T}$:

$$\Sigma := \sum_{k=-\infty}^{\infty} \mathrm{Cov}\big(\mathbf{g}_C(X_0, Y_0), \mathbf{g}_C(X_k, Y_k)\big). \tag{4}$$

The covariance matrix reflects the ICDF structure. Variances typically rise with the threshold, nearby moment conditions are strongly positively correlated, and fine grids often produce ill-conditioned covariance matrices with lower effective than nominal dimension. These features shape the behavior of the test statistics below.

2.2 Structure of contact points

The SD conditions bind under the null at points where the integrated distribution functions $F^{(2)}(z)$ and $G^{(2)}(z)$ coincide locally, that is, where they touch without crossing. Such contacts arise trivially at the infimum of the joint support, $z_\star$, or over the entire support in the degenerate equality case $F = G$. A contact point may also occur at the supremum of the support, where the SD condition reduces to the means inequality $\mathbb{E}[X_t] \geq \mathbb{E}[Y_t]$, with binding when $\mathbb{E}[X_t] = \mathbb{E}[Y_t]$.

To characterize *interior* contact points, we assume in this subsection that F and G are continuously differentiable on the interior of $\mathcal{Z}$, with densities f and g, so that Δ is twice continuously differentiable on $\text{int}(\mathcal{Z})$. This smoothness requirement is not an arbitrary restriction imposed directly on the ICDF gap, because the gap cannot be specified freely: it is an antiderivative of the CDF difference. On $\text{int}(\mathcal{Z})$, $\Delta'(z) = G(z) - F(z)$ and, where densities exist, $\Delta''(z) = g(z) - f(z)$. Hence an interior contact point z_0 can occur only if $\Delta(z_0) = 0$ and $\Delta'(z_0) = G(z_0) - F(z_0) = 0$. Thus the two integrated distribution functions must touch at z_0 without crossing. This is a double-root condition for the ICDF gap and is non-generic in bottom-up distributional constructions: small perturbations of either underlying distribution typically remove the equality or convert it into isolated slack or violated inequalities.

The same derivative structure explains why continuous sets of informative contacts are exceptional. If $\Delta(z) = 0$ on a nontrivial interval I, then necessarily $G(z) = F(z)$ for all $z \in I$, and, where densities exist, $g(z) = f(z)$ throughout I. A flat contact interval therefore requires exact equality of the two distributions over that interval, together with the appropriate boundary condition for the ICDF gap. Such configurations can be imposed abstractly at the level of the inequality function, but they do not arise generically from distribution functions whose ICDFs are linked as antiderivatives of CDFs. Degenerate equality cases, including $F = G$, generate contact over the support but are uninformative for detecting dominance violations.

Consequently, in generic smooth settings the set of informative binding SD constraints is either empty or finite. Multiple informative contacts may nevertheless arise by construction, for example from optimization over mixtures of distributions subject to SD constraints, where the objective function or auxiliary constraints explicitly favor or require several binding points. In applied economic settings, however, the emergence of interior contacts remains constrained by the distributional origin of the ICDF gap and by side constraints that often render SD inequalities slack.

When interior binding SD constraints do occur, they correspond generically to isolated strict local minima of the SD functional $\Delta(z)$. At such a contact point z_0, one has $\Delta(z_0) = 0$, $\Delta'(z_0) = 0$, and, in the regular case, $\Delta''(z_0) > 0$. Non-isolated informative contact sets require flat-contact degeneracies, while isolated but non-strict contact points require higher-order tangency, such as $\Delta(z_0) = \Delta'(z_0) = \Delta''(z_0) = 0$. These cases impose knife-edge restrictions and are unstable under small perturbations of the underlying distributions. We therefore focus on the regular case of finitely many isolated strict local minima, which is sufficient for regular identification and chi-bar-square asymptotic behavior of the proposed test statistics.

2.3 Test procedures

2.3.1 LMW test

The one-sided KS statistic is defined as $\mathrm{LMW}_T := \sqrt{T}\sup_{z\in\mathcal{Z}_{T,\infty}} -\Delta_T(z)$. Subsamples of size $b^{(L)} = b_T^{(L)}$ are used to construct the empirical distribution of the statistic. The subsample length b_T is a test parameter satisfying $b_T^{(L)} \to \infty$ and $b_T^{(L)}/T \to 0$, typically chosen by a rule of thumb such as $b_T^{(L)} \approx T^{0.5\text{–}0.7}$.

For IID data, subsamples may be drawn randomly without replacement from the full sample; in this case, the number of subsamples B_T is a user-chosen MC parameter satisfying $B_T \to \infty$, and is taken sufficiently large in practice, e.g., several hundred or thousand, to accurately approximate the subsampling distribution. For serially dependent data, subsamples should consist of consecutive observations to preserve the dependence structure, in which case the number of subsamples is typically $B_T = T - b_T^{(L)} + 1$ when all overlapping blocks are used.

For each subsample $\mathcal{I}_{k,b_T^{(L)}} := \{k, \cdots, k + b_T^{(L)} - 1\}$, $k = 1, \ldots, B_T$, compute

$$\mathrm{LMW}_{k,b_T^{(L)}} := \sqrt{b_T^{(L)}} \sup_{z \in \mathcal{Z}_{T,\infty}} -\Delta_{k,b_T}(z), \qquad \Delta_{k,b_T^{(L)}}(z) := \frac{1}{b_T^{(L)}} \sum_{s \in \mathcal{I}_{k,b_T^{(L)}}} g_z(X_s, Y_s).$$

When re-centered subsampling is employed, the subsample statistics are constructed from the deviation of the subsample moment curve from the full-sample moment curve, $\tilde{\Delta}_{k,b_T^{(L)}}(z) = \Delta_{k,b_T^{(L)}}(z) - \Delta_T(z)$. Let $\hat{q}_{1-\alpha}$ be the empirical $(1-\alpha)$ quantile of $\{\mathrm{LMW}_{k,b_T}\}_{k=1}^{B_T}$. The test rejects the null hypothesis H_0 if $\mathrm{LMW}_T > \hat{q}_{1-\alpha}$.

The test is not self-normalizing: the test statistic scales with the block size, and sample variability is accounted for only through subsampling. By construction, the method accommodates serial dependence via consecutive subsamples, while IID subsampling is a special case. The choice of $b_T^{(L)}$ balances bias and variance: small $b_T^{(L)}$ gives noisy quantiles, while large $b_T^{(L)}$ may smooth over violations of the null.

2.3.2 LSW test

Let ν_T be a discrete positive measure supported on the implemented constraint set $\mathcal{Z}_{T,\infty}$, with weights $w_{T,j} \geq 0$. Writing $\mathcal{Z}_{T,\infty} = \{z_{T,1}, \ldots, z_{T,m_{T,\infty}}\}$, the LSW test statistic is $\mathrm{LSW}_T := T \sum_{j=1}^{m_{T,\infty}} w_{T,j} [-\Delta_T(z_{T,j})]_+^2$, where $[-\Delta_T(z)]_+ := \max\{-\Delta_T(z), 0\}$ measures the violation of the moment inequality.

To focus on potentially binding constraints, define the trimming sequence $c_T = c_0 \log(\log T) T^{-1/2}$

and the empirical contact set $\widehat{C}_T(c_T) := \{z \in \mathcal{Z}_{T,\infty} : |\Delta_T(z)| < c_T\}$. Define the index set

$$J_T := \begin{cases} \{j : z_{T,j} \in \widehat{C}_T(c_T)\}, & \text{if } \widehat{C}_T(c_T) \neq \emptyset, \\ \{1, \dots, m_{T,\infty}\}, & \text{otherwise.} \end{cases}$$

For the bootstrap, draw pseudo-samples $\{X_t^*, Y_t^*\}_{t=1}^T$ with replacement from the original data $\{X_t, Y_t\}_{t=1}^T$ and define $\Delta_T^*(z) := T^{-1} \sum_{t=1}^T g_z(X_t^*, Y_t^*)$. Re-center using the original sample gaps, $\Delta_T^*(z) - \Delta_T(z)$. The bootstrap statistic is then

$$\mathrm{LSW}_T^* := T \sum_{j \in J_T} w_{T,j} [-(\Delta_T^*(z_{T,j}) - \Delta_T(z_{T,j}))]_+^2.$$

Let $\hat{q}_{1-\alpha}$ denote the empirical $(1-\alpha)$ quantile of $\{\mathrm{LSW}_T^*\}$. Reject H_0 if $\mathrm{LSW}_T > \hat{q}_{1-\alpha}$.

The LSW procedure is originally developed for IID data. For dependent data, draw a block-bootstrap pseudo-sample with block length b_T satisfying $b_T \to \infty$ and $b_T/T \to 0$. LSW is not self-normalizing in the sense that the variance of $[-\Delta_T(z)]_+^2$ is not explicitly normalized, using studentization or otherwise; the bootstrap distribution accounts for finite-sample variability.

The trimming sequence c_T is intended to focus the statistic on inequalities that are close to binding. In applications, however, c_0 must be chosen before observing the rejection frequency of the test. We therefore treat c_0 as an implementation constant and examine the sensitivity of the feasible LSW procedure to nearby values of this constant. This sensitivity analysis is diagnostic: it evaluates the stability of the trimming rule, but it is not a feasible rule for selecting c_0 ex post to match nominal size.

2.3.3 ELR test

We describe the ELR test procedure in six implementation steps.

Step 1: Block construction. Let the block length $\ell = \ell_T$ satisfy $\ell_T \to \infty$ and $\ell_T/T \to 0$.

Define overlapping block averages

$$\bar{g}_{s,\ell}(z) := \frac{1}{\ell}\sum_{t=s}^{s+\ell-1} g_z(X_t, Y_t), \qquad s = 1, \ldots, T_\ell, \qquad T_\ell = T - \ell + 1. \tag{5}$$

For IID data, one may set $\ell = 1$, in which case the procedure reduces to the standard observation-level ELR. For serially dependent data, the block averages provide moment observations that preserve local dependence at the scale determined by ℓ.

Step 2: Localization of candidate binding constraints. We localize candidate binding constraints using a relaxed notion of a local minimizer for the empirical ICDF gap function. Let $d = d_T$ be a localization sequence with $d_T \downarrow 0$ and $\sqrt{T} d_T \to \infty$. When the mean restriction is imposed, set $\widehat{C}_{T,\infty} := \infty$ if $\Delta_T(\infty) \leq d_{T,\infty}$ and $\widehat{C}_{T,\infty} := \emptyset$ otherwise, where $d_{T,\infty} \downarrow 0$ and $\sqrt{T} d_{T,\infty} \to \infty$. If the mean restriction is not imposed, set $\widehat{C}_{T,\infty} := \emptyset$. Define

$$\widehat{C}_T := \{z \in \mathcal{Z}_T : z \text{ is a local minimum of } \Delta_T(\cdot); \Delta_T(z) \leq d_T\} \cup \widehat{C}_{T,\infty}. \tag{6}$$

A grid point $z_{T,i}$, $i = 2, \ldots, m_T - 1$, is a local minimum if $\Delta_T(z_{T,i}) \leq \Delta_T(z_{T,i-1})$ and $\Delta_T(z_{T,i}) \leq \Delta_T(z_{T,i+1})$. The endpoint $z_{T,1}$ is a local minimum if $\Delta_T(z_{T,1}) \leq \Delta_T(z_{T,2})$, and z_{T,m_T} is a local minimum if $\Delta_T(z_{T,m_T}) \leq \Delta_T(z_{T,m_T-1})$.

The localization rule has two components. For finite threshold constraints, it restricts attention to local minima of the empirical ICDF gap; it then applies the one-sided level condition $\Delta_T(z) \leq d_T$, which excludes empirical local minima that are clearly slack. The one-sided level condition is important: positive slack constraints are removed asymptotically, while negative empirical constraints remain eligible for selection, preserving consistency against fixed alternatives.

All moment vectors are restricted to $\widehat{C}_T$, and the same localized set is used in all bootstrap replications. If $\widehat{C}_T = \emptyset$, the full-sample and bootstrap ELRs are set equal to zero, corresponding to the strictly slack case in which no candidate binding constraint is selected.

This localization rule does not require second derivatives or exact empirical binding.

Under local strict convexity of the population gap $\Delta(z)$, each binding point is isolated, and the empirical rule selects grid points in vanishing neighborhoods of the true binding points as $\mathcal{Z}_T$ becomes dense and d_T shrinks. Multiple nearby empirical minima generated by local flatness of $\Delta_T(z)$ are asymptotically collinear and span the same linear space of constraint gradients, so over-selection does not affect the limiting tangent cone. In finite samples, possible power loss from over-selection can be reduced by local quadratic-growth filters, pre-localization smoothing with a vanishing bandwidth, or post-selection clustering of highly correlated adjacent minima, for example using a threshold such as $\rho_T = 1 - T^{-2/3}$. Thus, unlike LMW, which uses all grid points, or LSW, which uses global trimming, ELR selects structurally relevant local minima as candidate binding constraints.

Step 3: Full-sample ELR. Let $\bar{\mathbf{g}}_{s,\ell}$ denote the vector of block moment averages over $z \in \widehat{C}_T$ for block $s = 1, \ldots, T_\ell$. The blockwise EL is defined as

$$\mathcal{L}_B = \max \left\{ \sum_{s=1}^{T_\ell} \log(p_s) : p_s \geq 0,\ \sum_{s=1}^{T_\ell} p_s = 1,\ \sum_{s=1}^{T_\ell} p_s\, \bar{\mathbf{g}}_{s,\ell} \geq 0 \right\}. \tag{7}$$

Let $\{p_s^\star\}_{s=1}^{T_\ell}$ denote the optimizer of this primal problem. The ELR is

$$\mathrm{ELR}_T := -2\frac{T}{T_\ell \ell} \sum_{s=1}^{T_\ell} \log(T_\ell p_s^\star). \tag{8}$$

The statistic is pointwise and self-normalizing. It can detect violations at localized threshold points without dilution from integration, retain joint evidence from several localized violations rather than only the most extreme coordinate, and adjust for threshold-specific variability through the EL geometry.

In practice, the dual formulation is computationally more convenient. Let $\widehat{\lambda}_T \leq 0$ denote the dual solution. Then

$$\mathrm{ELR}_T = 2\frac{T}{T_\ell \ell} \sum_{s=1}^{T_\ell} \log\Big(1 + \widehat{\lambda}_T^\top \bar{\mathbf{g}}_{s,\ell}\Big). \tag{9}$$

The feasibility condition $1 + \widehat{\lambda}_T^\top \bar{\mathbf{g}}_{s,\ell} > 0$ need not be imposed separately because interior-point or self-concordant barrier methods keep iterates strictly feasible. At the optimum, the primal inequality $\sum_{s=1}^{T_\ell} p_s \, \bar{\mathbf{g}}_{s,\ell} \geq 0$ is enforced through complementary slackness via $\widehat{\lambda}_T \leq 0$.

Step 4: Bootstrap pseudo-samples. Let B_T denote the number of bootstrap replications. For each replication $k = 1, \ldots, B_T$, generate a bootstrap pseudo-sample $\{(X_{k,t}^*, Y_{k,t}^*)\}_{t=1}^T$ from the original sample. For IID data, this is the ordinary nonparametric bootstrap. For serially dependent data, the pseudo-sample is generated by a block bootstrap to preserve dependence, using bootstrap block size equal to b_T. The localized set $\widehat{C}_T$ selected in Step 2 is kept fixed across all bootstrap replications.

Step 5: Re-centered EL on bootstrap pseudo-samples. For each bootstrap pseudo-sample, construct block averages over the localized set $\widehat{C}_T$:

$$\bar{g}_{k,r,\ell}^*(z) = \frac{1}{\ell} \sum_{t=r}^{r+\ell-1} g_z(X_{k,t}^*, Y_{k,t}^*), \qquad r = 1, \ldots, T_\ell. \tag{10}$$

Let $\Delta_T(\widehat{C}_T)$ denote the vector of full-sample moment averages over the localized set. Define the re-centered bootstrap block moments $\widetilde{\mathbf{g}}_{k,r,\ell}^* = \bar{\mathbf{g}}_{k,r,\ell}^*(\widehat{C}_T) - \Delta_T(\widehat{C}_T)$. Compute the bootstrap EL problem

$$\mathcal{L}_{k,T}^* = \max \left\{ \sum_{r=1}^{T_\ell} \log(p_r) : p_r \geq 0, \; \sum_{r=1}^{T_\ell} p_r = 1, \; \sum_{r=1}^{T_\ell} p_r \, \widetilde{\mathbf{g}}_{k,r,\ell}^* \geq 0 \right\}. \tag{11}$$

The inequality direction is the same as in the full-sample EL problem. Re-centering places the bootstrap moments on the estimated boundary of the null but does not change the sign of the dominance restriction, so the bootstrap EL problem continues to impose the nonnegative moment cone.

Let $\mathrm{ELR}_{k,T}^*$ denote the corresponding bootstrap ELR:

$$\mathrm{ELR}_{k,T}^* := -2 \frac{T}{T_\ell \ell} \sum_{r=1}^{T_\ell} \log(T_\ell p_{k,r}^\star), \tag{12}$$

where $\{p_{k,r}^\star\}_{r=1}^{T_\ell}$ denotes the optimizer of the bootstrap EL problem. By centering the pseudo-sample moments around zero on the localized candidate binding set, the bootstrap distribution mimics the Gaussian boundary experiment governing the limiting null distribution of the localized ELR.

Step 6: Bootstrap distribution and decision rule. Define the conditional bootstrap distribution by

$$\widehat{F}_T^*(x) = \frac{1}{B_T} \sum_{k=1}^{B_T} \mathbf{1}\{\text{ELR}_{k,T}^* \leq x\}. \tag{13}$$

Let $\widehat{c}_{\alpha,T}^* = (\widehat{F}_T^*)^{-1}(1-\alpha)$ denote the bootstrap critical value. The null hypothesis H_0 is rejected if $\text{ELR}_T > \widehat{c}_{\alpha,T}^*$.

In some applications, prior information about the relationship between X and Y may imply that the finite population contact set contains at most one non-trivial contact point. This occurs, for example, in the simulation experiment when Y is the stock index and X is an enhanced index based on a single short call condor spread. In such cases, the bootstrap calibration above may be replaced by the scalar boundary limit when the unique possible contact is binding. Specifically, the ELR null limit is $\frac{1}{2}\chi_0^2 + \frac{1}{2}\chi_1^2$, so the level-$\alpha$ asymptotic critical value is the $(1-2\alpha)$ quantile of a χ_1^2 distribution. If the dominance inequalities are strictly slack, the statistic degenerates at zero, so this critical value is conservative.

3 Statistical Theory

This section establishes the asymptotic properties of the proposed procedures and develops the local asymptotic theory that explains their comparative behavior. The first-order theory is presented concisely, since its main role is to justify the validity of the testing procedures and to reduce the original continuum of SSD inequalities to a finite-dimensional problem on the relevant contact set. Detailed assumptions, auxiliary lemmas, and proofs are collected in the supplement.

The key statistical issue is the behavior of the empirical local minima of the ICDF gap. Under the null hypothesis, the informative binding constraints are the non-trivial contact points of the population gap function. The proposed localization rule estimates these points by selecting empirical local minima whose empirical gaps are sufficiently close to zero. The first-order theory shows that this localized set converges to the population contact set and that, after localization, the three testing procedures admit Gaussian limits on the same finite-dimensional contact space.

The local power analysis then studies how the three statistics transform this common Gaussian object into rejection regions. This is where the procedures differ. LMW uses an extremal functional, LSW aggregates squared negative parts, whereas ELR uses a self-normalized cone projection. The resulting Gaussian-cone geometry explains why ELR can exploit covariance features of multiple binding constraints and why its advantages are intrinsically multidimensional. Throughout, $\rightsquigarrow$ denotes convergence in distribution.

3.1 First-order asymptotic properties

The asymptotic analysis is conducted under the following assumptions. Their detailed discussion, proofs and all auxiliary results are provided in the Supplement. Let $C = \{c_1, \ldots, c_J\} \subset \mathcal{Z}_\infty$ denote the non-trivial population contact set under the null. If $J > 0$, write

$$g_C(X_t, Y_t) = \big(g_{c_1}(X_t, Y_t), \ldots, g_{c_J}(X_t, Y_t)\big)^\top$$

and let

$$\Sigma = \sum_{k=-\infty}^{\infty} \mathrm{Cov}\{g_C(X_0, Y_0), g_C(X_k, Y_k)\}$$

be the corresponding long-run covariance matrix.

Assumption 3.1 (Regularity conditions)**.** *The following hold:*

(A1) The process $\{(X_t, Y_t)\}_{t\in\mathbb{Z}}$ is strictly stationary and absolutely regular (β-mixing), with $\beta(k) \le Ck^{-(1+\epsilon)}$, $k \ge 1$, for some constants $C < \infty$ and $\epsilon > 0$.

(A2) There exist $\delta \ge 1$ and $C^\star < \infty$ such that $\mathbb{E}|X_t|^{2+\delta} + \mathbb{E}|Y_t|^{2+\delta} \le C^\star$, with $\epsilon > 2 + \frac{4}{\delta}$.

(A3) The finite set of strict local minima of Δ *on* $\mathcal{Z}$*, for which* $\Delta \leq 0$*, is denoted by* $\mathcal{C}_{\ell,f} = \{c_1^\star, \dots, c_{J_{\ell,f}}^\star\} \subset \mathcal{Z}$*. Also, for each* j *there exist* $r_j > 0$ *and* $\kappa_j > 0$ *such that on the neighborhood* $N_j := (c_j^\star - r_j, c_j^\star + r_j) \cap \mathcal{Z}$*,* $\Delta(z) - \Delta(c_j^\star) \geq \kappa_j (z - c_j^\star)^2$*,* $z \in N_j$*. When the mean restriction is imposed, the possible contact or violation at* ∞ *is handled separately through* $\Delta(\infty)$ *and* g_∞*. Under the null hypothesis, the full contact set is* $C = C_f \cup C_\infty$*, and* $J = |C|$*; if* $J > 0$*,* Σ *is positive definite.*

(A4) There exists a deterministic sequence $R_T \uparrow \infty$ *such that:*

- *(i) (*PK convergence on compacts*)* $\mathcal{Z}_T \cap [-R_T, R_T] \xrightarrow{p} \mathcal{Z} \cap [-R_T, R_T]$ *in the Painlevé–Kuratowski (PK) topology;*
- *(ii) (*Local density around finite contacts*) writing* $C_f = \{c_{f,1}, \dots, c_{f,J_f}\}$*, for each* $j = 1, \dots, J_f$, $\mathrm{dist}(c_{f,j}, \mathcal{Z}_T) := \inf_{z \in \mathcal{Z}_T} |z - c_{f,j}| \xrightarrow{p} 0$.

Assumption 3.1 separates the probabilistic and geometric ingredients underlying the asymptotic analysis.

Conditions (A1)–(A2) provide the stochastic regularity required for the empirical ICDF gap process. In particular, they guarantee the existence of the long-run covariance kernel associated with the SSD moment class and imply a functional central limit theorem for the empirical gap process over the threshold space. Consequently, the asymptotic fluctuations of the empirical gap are described by a tight Gaussian process.

Conditions (A3)–(A4) govern the geometry of the population ICDF gap and the consistency of the localization procedure. The local quadratic separation assumption ensures that each relevant contact point is isolated and therefore admits a unique empirical counterpart asymptotically. Together with the consistency of the threshold grid, this implies that the empirical local minimizers selected by the localization algorithm converge to the corresponding population contact points in the Painlevé–Kuratowski topology.

The combined effect of these assumptions is that the original continuum of SSD inequalities is asymptotically reduced to a finite-dimensional Gaussian experiment supported on the contact set. This reduction forms the basis of both the localized empirical likelihood construction and the local-power analysis developed in the remainder of this section.

When the mean restriction is imposed, the possible contact at infinity is treated separately through $\Delta(\infty)$ and the corresponding moment function g_∞, without affecting the finite-dimensional reduction.

The following theorem collects the first-order asymptotic properties of the three procedures.

Theorem 3.1 (First-order asymptotic properties)**.** *Suppose Assumption 3.1 holds.*

(i) Localization and reduction of the statistical experiment. *Under the null hypothesis, if $J > 0$, the localized empirical contact set $\widehat{C}_T$ converges in probability to the population contact set C in the Painlevé–Kuratowski topology. Consequently, every population contact point admits an asymptotically unique empirical counterpart, whereas asymptotically inactive inequalities are discarded with probability tending to one.*

(ii) Null limits. *Let $\mathbb{G}$ denote the tight mean-zero Gaussian limit of the empirical ICDF gap process. Then, under $\mathbf{H}_0$, and if*

$$\mathrm{LMW}_T \rightsquigarrow \sup_{z\in C}\big[-\mathbb{G}(z)\big], \quad \mathrm{LSW}_T \rightsquigarrow \int_C \big[-\mathbb{G}(z)\big]_+^2 \,\nu(dz),$$

where ν denotes the limiting contact measure. Moreover, if $\ell_T \to \infty$, $\ell_T T^{1/(2+\delta)-1/2} \to 0$, then

$$\mathrm{ELR}_T \rightsquigarrow Q(\Sigma) := \inf_{\eta\in\mathbb{R}_+^J} (W-\eta)^\top \Sigma^{-1}(W-\eta), \qquad W \sim N(0,\Sigma).$$

Equivalently, the localized ELR statistic converges to a $\bar{\chi}^2$ distribution whose weights are determined by the covariance matrix Σ.

(iii) Pitman local alternatives.

Under local alternatives satisfying $\Delta_T^{(h)}(z) := \Delta(z) + T^{-1/2}h(z), \quad z \in \mathcal{Z}_\infty$,

$$\mathrm{LMW}_T \rightsquigarrow \sup_{z\in C}\big[-\{\mathbb{G}(z)+h(z)\}\big], \quad \mathrm{LSW}_T \rightsquigarrow \int_C \big[-\{\mathbb{G}(z)+h(z)\}\big]_+^2 \,\nu(dz),$$

and if $\ell_T \to \infty$, $\ell_T T^{1/(2+\delta)-1/2} \to 0$,

$$\mathrm{ELR}_T \rightsquigarrow \inf_{\eta \in \mathbb{R}_+^J} (W + \mu_h - \eta)^\top \Sigma^{-1} (W + \mu_h - \eta),$$

where $\mu_h = \big(h(c_1), \ldots, h(c_J)\big)^\top$. *Hence, local alternatives modify the limiting experiment only through a deterministic translation of the common Gaussian limit on the contact set, yielding a finite-dimensional Gaussian shift experiment.*

(iv) Asymptotic validity. *The subsampling critical values for LMW and the bootstrap critical values for LSW consistently estimate the corresponding limiting quantiles whenever the relevant localization or trimming rules are asymptotically correct. The same holds for the localized ELR boostrap critical values if* $\ell_T \to \infty$, $\ell_T T^{1/(2+\delta)-1/2} \to 0$, *and* $b_T \to \infty$, $b_T/T \to 0$, $\ell_T/b_T \to 0$. *Consequently, all three procedures are asymptotically exact whenever the contact set is nonempty (*$J > 0$*), whereas under strict slackness (*$J = 0$*) the limiting statistics degenerate and the resulting procedures become asymptotically conservative.*

(v) Fixed alternatives. *If* $\inf_{z \in \mathcal{Z}_\infty} \Delta(z) < 0$, *then the three statistics diverge in probability, whereas the corresponding critical values remain bounded in probability. Consequently, the LMW, LSW and localized ELR procedures are all consistent against fixed alternatives.*

Theorem 3.1 provides the common first-order asymptotic foundation for the three testing procedures. Its central conclusion is that localization preserves all first-order statistical information while eliminating asymptotically inactive inequalities. As a result, the original continuum of stochastic dominance inequalities is asymptotically reduced to a finite-dimensional Gaussian experiment supported on the contact set.

This reduction has two important consequences. First, it establishes the asymptotic validity of the localized LMW, LSW and ELR procedures under weak dependence, including their limiting null distributions, validity of the corresponding calibration schemes, and consistency against fixed alternatives. Second, because all three procedures are driven by the same Gaussian experiment after localization, their asymptotic differences cannot originate from the underlying empirical process itself. They arise solely from the different ways in which the three statistics transform the common Gaussian limit into rejection regions.

The remainder of this section therefore focuses on this geometric aspect of the problem. By studying the Gaussian shift experiment induced by Pitman alternatives and the geometry of the corresponding rejection boundaries, we characterize the corresponding local-power properties and explain the distinct role played by covariance information in the localized empirical likelihood approach.

3.2 Local asymptotic power

We now compare the three tests under local alternatives. By Theorem 3.1, after localization the relevant asymptotic experiment is finite-dimensional and is supported on the population contact set $C = \{c_1, \ldots, c_J\}$. Local power comparisons are thus carried out by studying how the limiting rejection regions of the size corrected procedures behave under Gaussian shifts.

Let $\widehat{\mathbf{g}}_T := \sqrt{T}\big(\widehat{\Delta}_T(c_1), \ldots, \widehat{\Delta}_T(c_J)\big)^\top$. Under the null hypothesis, $\widehat{\mathbf{g}}_T \rightsquigarrow W$, $W \sim N(0, \Sigma)$. Under Pitman alternatives with contact-restricted drift $\mu_h := \big(h(c_1), \ldots, h(c_J)\big)^\top$, the limiting experiment becomes $\widehat{\mathbf{g}}_T \rightsquigarrow W + \mu_h$, $W \sim N(0, \Sigma)$. Dominance-violating local alternatives correspond to drift vectors satisfying $\mu_{h,j} \leq 0$ for all j, with strict inequality for at least one contact coordinate.

Let $\Psi : \mathbb{R}^J \to \mathbb{R}$ denote the limiting statistic of a size-corrected test, and let c_α be the corresponding $(1-\alpha)$-critical value under $W \sim N(0, \Sigma)$. The limiting rejection region is $\mathcal{R}_\Psi := \{w \in \mathbb{R}^J : \Psi(w) > c_\alpha\}$. For a scalar local-intensity parameter $t \geq 0$, define the limiting local power function $\pi_\Psi(t; h) := \mathbb{P}\{\Psi(W + t\mu_h) > c_\alpha\}$. The following result gives a common expansion for the local power functions of all three tests.

Theorem 3.2 (Gaussian shift expansion)**.** *Let $W \sim N(0, \Sigma)$, where Σ is positive definite. Suppose that $\mathbb{P}\{\Psi(W) = c_\alpha\} = 0$, that $\mathcal{R}_\Psi$ is open with Lipschitz boundary $\partial\mathcal{R}_\Psi$, and that* *the outward unit normal $n(w)$ exists for $\mathcal{H}_{J-1}$-almost every $w \in \partial\mathcal{R}_\Psi$. Suppose also that the Gaussian surface integrals below are finite. Then, as $t \downarrow 0$,*

$$\pi_\Psi(t;h) = \alpha + t\,\pi_\Psi^{(1)}(h) + \frac{t^2}{2}\,\pi_\Psi^{(2)}(h) + o(t^2),$$

where

$$\pi_\Psi^{(1)}(h) = \mathbb{E}\big[\mu_h^\top \Sigma^{-1} W\, \mathbf{1}\{W \in \mathcal{R}_\Psi\}\big]$$

and

$$\pi_\Psi^{(2)}(h) = \mathbb{E}\Big[\big(\mu_h^\top \Sigma^{-1} W\big)^2 \mathbf{1}\{W \in \mathcal{R}_\Psi\}\Big] - \big(\mu_h^\top \Sigma^{-1} \mu_h\big)\alpha.$$

Equivalently, the first two derivatives admit the (Stein) boundary representations

$$\pi_\Psi^{(1)}(h) = -\int_{\partial\mathcal{R}_\Psi} \mu_h^\top n(w)\,\varphi_\Sigma(w)\,d\mathcal{H}_{J-1}(w),$$

and

$$\pi_\Psi^{(2)}(h) = -\int_{\partial\mathcal{R}_\Psi} \{\mu_h^\top n(w)\}\{\mu_h^\top \Sigma^{-1} w\}\varphi_\Sigma(w)\,d\mathcal{H}_{J-1}(w),$$

where φ_Σ denotes the $N(0,\Sigma)$ density.

The theorem shows that local power is governed by the interaction between the drift direction μ_h, the Gaussian density, and the outward normals of the limiting rejection boundary. The three tests differ precisely through this boundary geometry. LMW has coordinatewise flat faces, LSW has curved coordinate-aggregation boundaries, while ELR has a cone-projection boundary determined by the covariance matrix Σ.

When comparing two size-corrected tests A and B, we say that A is locally more powerful than B in direction h if the derivative sequence $\big(\pi_A^{(1)}(h), \pi_A^{(2)}(h), \ldots\big)$ is lexicographically larger than $\big(\pi_B^{(1)}(h), \pi_B^{(2)}(h), \ldots\big)$. In the generic case the first derivative already determines the comparison. Higher-order derivatives matter only when lower-order responses coincide.

3.2.1 Applications to LMW, LSW and ELR

We next apply Theorem 3.2 to the three limiting statistics. The corollaries below make explicit how each procedure converts the same Gaussian shift experiment into local power.

Corollary 3.1 (Local power of LMW). *Let* $\Psi_{\text{LMW}}(w) = \sup_{1\le j\le J}(-w_j) = -\min_{1\le j\le J} w_j$*, and let* c_{LMW} *be its* $(1-\alpha)$*-critical value under* $W \sim N(0,\Sigma)$*. Then* $\mathcal{R}_{\text{LMW}} = \{w : \min_{1\le j\le J} w_j < -c_{\text{LMW}}\}$*. Its boundary is the union, up to Hausdorff-null intersections, of the coordinate faces* $\partial\mathcal{R}^{(j)}_{\text{LMW}} := \{w : w_j = -c_{\text{LMW}},\ w_k \ge -c_{\text{LMW}} \text{ for all } k \neq j\}$*,* $j = 1,\dots,J$*. The outward unit normal on the* j*-th face is* $n^{(j)} = e_j$*. Therefore,*

$$\pi^{(1)}_{\text{LMW}}(h) = -\sum_{j=1}^{J} \mu_{h,j} \int_{\partial\mathcal{R}^{(j)}_{\text{LMW}}} \varphi_\Sigma(w)\, d\mathcal{H}_{J-1}(w),$$

and

$$\pi^{(2)}_{\text{LMW}}(h) = -\sum_{j=1}^{J} \mu_{h,j} \int_{\partial\mathcal{R}^{(j)}_{\text{LMW}}} \{\mu_h^\top \Sigma^{-1} w\}\varphi_\Sigma(w)\, d\mathcal{H}_{J-1}(w).$$

Corollary 3.1 shows that LMW reacts through coordinatewise boundary faces. Its first-order local power is a weighted sum of the negative drift components, where the weights are the Gaussian surface masses of the corresponding coordinate faces. Hence LMW is naturally sensitive to sparse violations concentrated on a single contact point.

Corollary 3.2 (Local power of LSW). *Let* $\Psi_{\text{LSW}}(w) = \sum_{j=1}^{J} a_j[-w_j]_+^2, \qquad a_j > 0$*, and let* c_{LSW} *be its* $(1-\alpha)$*-critical value under* $W \sim N(0,\Sigma)$*. Then* $\mathcal{R}_{\text{LSW}} = \left\{w : \sum_{j=1}^{J} a_j[-w_j]_+^2 > c_{\text{LSW}}\right\}$*. For each nonempty* $S \subset \{1,\dots,J\}$*, define the active-coordinate boundary stratum* $\partial\mathcal{R}_{\text{LSW}}(S) := \left\{w : w_j < 0\ (j \in S),\quad w_j \ge 0\ (j \notin S),\quad \sum_{j\in S} a_j w_j^2 = c_{\text{LSW}}\right\}$*. Up to Hausdorff-null intersections,* $\partial\mathcal{R}_{\text{LSW}} = \bigcup_{\emptyset\neq S\subset\{1,\dots,J\}} \partial\mathcal{R}_{\text{LSW}}(S)$*, and on* $\partial\mathcal{R}_{\text{LSW}}(S)$*, the outward unit normal is* $n_{\text{LSW}}(w) = -\frac{(a_j w_j \mathbf{1}\{j\in S\})_{j=1}^{J}}{\left(\sum_{j\in S} a_j^2 w_j^2\right)^{1/2}}$*. Consequently,*

$$\pi^{(1)}_{\text{LSW}}(h) = -\sum_{\emptyset\neq S\subset\{1,\dots,J\}} \int_{\partial\mathcal{R}_{\text{LSW}}(S)} \mu_h^\top n_{\text{LSW}}(w)\, \varphi_\Sigma(w)\, d\mathcal{H}_{J-1}(w),$$

and

$$\pi^{(2)}_{\mathrm{LSW}}(h) = -\sum_{\emptyset\neq S\subset\{1,\dots,J\}} \int_{\partial\mathcal{R}_{\mathrm{LSW}}(S)} \{\mu_h^\top n_{\mathrm{LSW}}(w)\}\{\mu_h^\top \Sigma^{-1} w\}\varphi_\Sigma(w)\, d\mathcal{H}_{J-1}(w).$$

Thus LSW aggregates information over active sets of negative coordinates. Unlike LMW, whose rejection boundary consists of coordinatewise half-space faces, LSW has curved level sets and combines evidence from several contact points whenever several coordinates are locally negative. The aggregation, however, is determined by fixed weights a_j rather than by the covariance geometry of the moment vector.

Corollary 3.3 (Local power of localized ELR)**.** *Let $\Psi_{\mathrm{ELR}}(w) = \inf_{\eta\in\mathbb{R}^J_+}(w-\eta)^\top\Sigma^{-1}(w-\eta)$, and let c_{ELR} be its $(1-\alpha)$-critical value under $W \sim N(0,\Sigma)$. Define the whitened variable $v = \Sigma^{-1/2}w$, $\widetilde{\mu}_h = \Sigma^{-1/2}\mu_h$, and the covariance-induced oblique cone $K_\Sigma = \Sigma^{-1/2}\mathbb{R}^J_+$. Then the ELR limiting statistic can be written as $\Psi_{\mathrm{ELR}}(w) = \mathrm{dist}(v, K_\Sigma)^2$. Hence, in whitened coordinates, $\mathcal{R}_{\mathrm{ELR}} = \{v : \mathrm{dist}(v, K_\Sigma)^2 > c_{\mathrm{ELR}}\}$. Let $\Pi_{K_\Sigma}(v)$ denote Euclidean projection onto K_Σ, and set $r(v) = v - \Pi_{K_\Sigma}(v)$. At almost every boundary point, $\|r(v)\|^2 = c_{\mathrm{ELR}}$, and the outward unit normal is $n_{\mathrm{ELR}}(v) = -\frac{r(v)}{\sqrt{c_{\mathrm{ELR}}}}$. Therefore,*

$$\pi^{(1)}_{\mathrm{ELR}}(h) = \frac{1}{\sqrt{c_{\mathrm{ELR}}}} \int_{\partial\mathcal{R}_{\mathrm{ELR}}} \widetilde{\mu}_h^\top r(v)\, \varphi_I(v)\, d\mathcal{H}_{J-1}(v),$$

and

$$\pi^{(2)}_{\mathrm{ELR}}(h) = \frac{1}{\sqrt{c_{\mathrm{ELR}}}} \int_{\partial\mathcal{R}_{\mathrm{ELR}}} \{\widetilde{\mu}_h^\top r(v)\}\{\widetilde{\mu}_h^\top v\}\varphi_I(v)\, d\mathcal{H}_{J-1}(v),$$

where φ_I is the standard normal density on $\mathbb{R}^J$.

The ELR boundary is a fixed-distance surface around the cone $K_\Sigma = \Sigma^{-1/2}\mathbb{R}^J_+$. Thus its local power is controlled by the alignment between the whitened drift $\widetilde{\mu}_h$ and the projection residual $r(v)$, which is normal to the active face of the cone. Since the cone itself depends on Σ, ELR internalizes the covariance structure of the localized moment vector. This is the key distinction between ELR and the coordinate-based LMW and LSW procedures.

3.2.2 Geometric interpretation and comparison

The preceding corollaries reveal that the asymptotic local power differences arise entirely from the geometry of the limiting rejection regions induced by the corresponding test functionals. The essential geometric distinctions may be summarized as follows.

(i) The LMW rejection region is the union of coordinatewise half-spaces. Consequently, its local power depends exclusively on the Gaussian surface measure of coordinate faces and therefore reacts primarily to sparse local violations concentrated on individual contact points.

(ii) The LSW rejection region is determined by a weighted quadratic aggregation of the negative coordinates. Its local power therefore combines information across multiple contacts through Euclidean aggregation. This aggregation is determined by the prescribed weights and remains independent of the covariance structure of the localized moment vector.

(iii) The ELR rejection region is determined by the squared Mahalanobis distance to the covariance-induced cone $K_\Sigma = \Sigma^{-1/2}\mathbb{R}^J_+$. Consequently, its local power depends on the geometry of the projection onto K_Σ. After whitening, the covariance matrix determines the orientation of the cone itself, so that both the rejection boundary and its outward normal vectors are functions of the dependence structure of the localized moments.

The preceding comparison highlights the fundamentally different ways in which the three procedures utilize the information contained in the localized contact set. LMW measures departures through coordinatewise extrema and therefore ignores dependence between binding inequalities. LSW aggregates evidence over multiple contacts but does so through a fixed Euclidean geometry that is independent of the covariance structure. By contrast, ELR measures departures through Mahalanobis projection onto the covariance-induced cone. Consequently, its local sensitivity is determined jointly by the direction of the local drift and the covariance geometry of the binding inequalities, allowing the procedure to adapt to the dependence structure of the localized moment vector.

Scalar contact case ($J = 1$). When the contact set consists of a single binding inequality, the geometric distinctions described above disappear. Indeed, after size correction, the three limiting statistics are monotone transformations of the same scalar Gaussian variable and therefore induce identical rejection regions. Hence, any asymptotic efficiency differences between the three methods are intrinsically multidimensional and arise only when several binding inequalities are simultaneously present.

4 Monte Carlo Simulation Experiment

We design an MC experiment as a stylized but realistic application of SD testing to option-enhanced indexation. The comparison asks whether an index payoff augmented by an option overlay dominates the raw index, a setting in which contact points can be controlled through the option overlay structure.

The simulations use serially IID observations, to isolate the statistic-geometry comparison: LMW maps the contact-reduced empirical process into a supremum statistic, LSW into an integrated squared-violation statistic, and ELR into a self-normalized cone-quadratic statistic. Introducing serial dependence would alter the covariance matrix and the resampling method, and would require additional choices about the dynamic DGP, the conditional or unconditional interpretation of the dominance null, and dependence-preserving implementations for all methods.

The design is deliberately conservative for ELR. It uses only a small number of contact points, $J = 1, 2, 3$, although ELR tends to benefit from larger contact sets because it aggregates violations across constraints through a covariance-weighted quadratic form. In addition, the binding moment conditions exhibit strong positive dependence and heterogeneous variances, so that after prewhitening the binding directions are partially aligned and the effective dimension is reduced.

We report both feasible and infeasible results. Feasible critical values are estimated by subsampling for LMW and bootstrapping for LSW and ELR. In the infeasible, or oracle, case, critical values are taken from the simulated binding-null distribution, giving exact size and isolating the discriminatory content of the statistic from critical-value estimation error.

4.1 Simulation process

We model the scaled value of the stock index H years ahead, Y, as lognormally distributed, $\log(Y) = \mu_Y H + \sigma_Y \sqrt{H}\, Z$, with $Z \sim N(0,1)$. The continuously compounded, maturity-matched net interest rate is denoted by r. The parameter values are representative of monthly SPX returns under normal market conditions: $\mu_Y = 0.08$, $\sigma_Y^2 = 0.2^2$, $r = 0$, and $H = 1/12$.

The enhanced index is $X = Y + P(Y)$, where $P(Y)$ is the net profit from maturity-matched options written on the index. By varying the option strategy and net premium, we generate cases in which the informative SD constraints are slack, binding, or violated. The covariance matrix of the LPM conditions is strongly non-spherical: nearby thresholds are highly correlated and variances increase at higher thresholds.

The option overlay consists of one or more short call condor spreads added to the index. Each condor combines long and short calls with four strike prices $K_1 < K_2 < K_3 < K_4$ and premia $C(K)$. The profit of a single condor is $P(Y; K_1, K_2, K_3, K_4) := P_0(K_1, K_2, K_3, K_4) - \max(Y - K_1, 0) + \max(Y - K_2, 0) + \max(Y - K_3, 0) - \max(Y - K_4, 0)$, where $P_0(K_1, K_2, K_3, K_4) := (C(K_1) - C(K_2) - C(K_3) + C(K_4))e^{rH}$ is the net premium including interest.

A single condor generates at most one binding constraint, corresponding to one interior contact point. Multiple binding constraints are generated by combining condors. For J condors, the total profit is $P(Y) = \sum_{j=1}^{J} P(Y; K_{j,1}, K_{j,2}, K_{j,3}, K_{j,4})$ with total net premium $P_0 := \sum_{j=1}^{J} P_0(K_{j,1}, K_{j,2}, K_{j,3}, K_{j,4})$. The strike vectors $\{K_{j,i}\}$ therefore determine the contact locations and the possible slacks or violations.

For $J = 1, 2, 3$, the total net premium is $P_0 = 0.01\,J/3$. The central strikes are $(K_{1,2}, K_{1,3}) = (0.99, 1.01)$ for $J = 1$; $(0.99, 1.01)$ and $(1.05, 1.07)$ for $J = 2$; and $(0.93, 0.95)$, $(0.99, 1.01)$, $(1.05, 1.07)$ for $J = 3$. Payoffs are made symmetric by imposing $(K_{j,2} - K_{j,1}) = (K_{j,4} - K_{j,3})$, leaving only the outer strike ranges $(K_{j,4} - K_{j,1})$ to be chosen numerically.

Binding cases are generated by setting the lower-bound level to zero and choosing the outer strike ranges so that the resulting gap function is active at J contact points. Slack and violated cases are generated by setting $\Delta_0(T) > 0$ and $\Delta_0(T) < 0$, respectively. For size analysis, a single condor is used with $\Delta_0(T) = \frac{1}{2}\hat{\sigma}(x - y)T^{-1/2}$, so the design approaches the boundary from above at the $T^{-1/2}$ rate. For power analysis, three condors are used with $\Delta_0(T) = -\frac{1}{2}\hat{\sigma}(x - y)T^{-1/2}$, so the design approaches the boundary from below. This yields local alternatives at the $T^{-1/2}$ rate, as in standard moment-inequality asymptotics.

Since the lower-bound restriction on $\Delta(z)$ is imposed globally, the contact points are the points at which this restriction is active. Local alternatives can therefore be summarized by the contact-level violation vector. We write $v := -\mu_h \geq 0$ for the positive violation-drift vector, normalized to have average component one. Larger entries of v correspond to larger local violations at the associated binding inequalities.

We consider three drift configurations. The first, baseline specification is the parallel drift $v_1 = (1, 1, 1)'$. The second is $v_2 \propto \Sigma^{1/2}\mathbf{1} \approx (0.70, 1.06, 1.25)'$, normalized to have average component one; it produces a balanced reflected direction after whitening and is useful for studying covariance-balanced alternatives. The third is $v_3 \propto \Sigma^{-1/2}\mathbf{1} \approx (1.72, 0.73, 0.55)'$, also normalized to have average component one. This vector loads more heavily on the first contact coordinate, which has the largest contribution to ELR local power in the covariance configuration considered here. Thus v_3 is designed to be more favorable to ELR than the covariance-balanced vector v_2, while v_1 provides the neutral parallel benchmark.

For each v_i, $i = 1, 2, 3$, the three-condor strikes are constructed so that, relative to the baseline violated design, the active contact-point lower bounds in the resulting design have local levels proportional to $v_{i,j}\Delta_0(T)$, $j = 1, 2, 3$. In the violated cases $\Delta_0(T) < 0$, this generates local violations with relative magnitudes given by the components of v_i.

Figure 1 illustrates the simulation design by plotting the ICDF gap function for nine cases. The top row shows the local-slack null designs for $T = 300, 1000, 3000$, where the inequalities hold but the minimum slack is positive and of order $T^{-1/2}$. The middle row shows the binding designs with $J = 1, 2, 3$ contact points. The bottom row shows the violated $J = 3$ designs for $T = 300, 1000, 3000$, corresponding to the parallel contact-coordinate drift $v_1 = (1, 1, 1)'$. The alternative drift specifications v_2 and v_3 are used in the power experiments below. The chosen condor strike values for the nine cases are reported in Online Supplement Table 1.

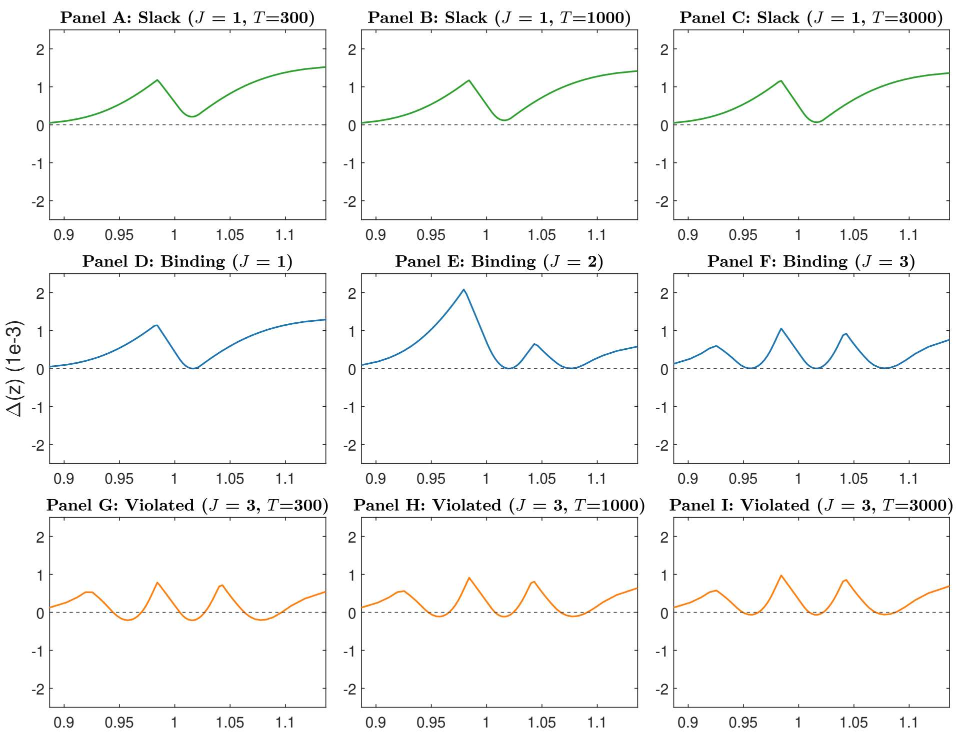

Figure 1: Simulation design. Each panel plots the ICDF gap $\Delta(z)$ for the corresponding index-plus-option overlay tested against the raw index.

4.2 Implementation details

For each DGP, we apply the naive benchmark, LMW, LSW, and ELR tests to 5000 MC samples with $T = 300, 1000$, and 3000. The null hypothesis is that the option-enhanced index (X) dominates the benchmark index (Y). All tests are applied to the same MC samples to reduce simulation noise in relative comparisons. A nominal significance level of 10% is used. In the oracle case, the critical value is the 90th percentile of the simulated null distribution under binding SD constraints. In the feasible case, critical values are estimated by resampling.

The feasible procedures require tuning constants for LMW subsampling, LSW trimming, ELR localization, and grid granularity. We fix a baseline implementation and report sensitivity to nearby choices as a finite-sample calibration diagnostic, not as an ex-post tuning rule.

To discretize the continuum of constraints, all tests use $m_T = \lfloor T^{m_0} \rfloor$ restrictions, $0 < m_0 < 1$. We define a regular grid on $[0, 1]$ by $p_{i,T} := i/m_T$, $i = 1, \ldots, m_T - 1$, and impose the ICDF inequality $\hat{F}^{(2)}(z_{i,T}) \leq \hat{G}^{(2)}(z_{i,T})$ at the corresponding quantiles $z_{i,T} := \hat{G}^{-1}(p_{i,T})$, $i = 1, \ldots, m_T - 1$, together with the means inequality $\mathbb{E}_{\hat{F}}[X] \geq \mathbb{E}_{\hat{G}}[Y]$. The baseline uses $m_0 = 0.6$, balancing data sparseness below the lowest threshold against the risk of missing violations between grid points. Robustness checks use $m_0 = 0.5$ and $m_0 = 0.7$.

Naive test. The naive benchmark treats the empirical CDFs as population CDFs and rejects whenever at least one empirical SD inequality is violated, without using a non-zero critical value. It therefore ignores sampling variation and provides an upper bound for the rejection rates of the statistical tests.

LMW test. We implement the LMW test described in 2.3.1 using the computer code appendix of Whang (2019), modified for our non-uniformly spaced constraint grid. We use centered IID subsampling, which performs better in the original study and in our application. For each MC sample, $B_T = 1000$ subsamples of size $b_T = \lfloor T^{b_0} \rfloor$ are used to estimate the distribution of the LMW statistic. The baseline uses $b_0 = 0.7$, with robustness checks for $b_0 \in \{0.6, 0.7, 0.8\}$. The IID subsampling assumption is favorable to LMW in the present serially IID design, although LSW and ELR similarly benefit from the absence of serial dependence.

LSW test. We implement the LSW test described in 2.3.2 using the computer code appendix of Whang (2019), again modified for the non-uniform grid. For each MC sample, 1000 IID bootstrap pseudo-samples approximate the distribution of LSW_T. Squared violations are equally weighted ($\{w_{T,j}\} = \{m_T^{-1}\}$). The trimming constant c_0 is fixed at $c_0 = 2^{-9}$ in the baseline and varied over $c_0 \in \{2^{-8}, 2^{-9}, 2^{-10}\}$ as a robustness diagnostic. The same baseline value is used in the main size and power comparisons.

ELR test. We implement the ELR test described in 2.3.3. Since the data are serially IID, the statistic is computed using individual observations ($\ell = 1$; $T_\ell = T$). Feasible critical values are obtained from pseudo-samples using the localization sequence $d_T(z) = d_0(T/\bar{T})^{1/3}\hat{\sigma}(g_z(X_t, Y_t))\bar{T}^{-1/2}$, where $\bar{T} = 3000$ is the largest sample size considered. This threshold accounts for threshold-specific sampling variability while satisfying the slow-shrinking localization requirement discussed in Section 2.3.3. The baseline fixes $d_0 = 2$ before the power comparisons and uses it uniformly across baseline tables; $d_0 = 1$ and $d_0 = 3$ are reported only as robustness diagnostics. The number of pseudo-samples is the same as for LMW and LSW.

4.3 Simulation results

Tables 1–2 report the main MC rejection rates, while Tables A.1–A.4 provide implementation diagnostics. For the Slack and Binding specifications, rejection rates measure empirical size at the nominal 10 percent level. For the Violated specifications, they measure power. We report both feasible power, based on estimated critical values, and infeasible size-adjusted power, based on the 90th percentile of the simulated Binding (3) null distribution. The infeasible benchmark isolates the discriminatory content of each statistic from critical-value estimation error.

Baseline size and power. The naive benchmark illustrates why formal critical values are needed. With one binding restriction, its rejection rate is close to 50 percent; with several binding restrictions, it rises above 50 percent but remains below one because nearby empirical gaps are strongly positively correlated. Thus sampling variation alone can generate apparent violations under binding nulls.

Among the formal tests, rejection rates are close to zero in the local-slack design, so the binding designs are more informative for size. With one binding constraint, ELR is essentially exact, while LMW and LSW are conservative. With two or three binding constraints, LMW remains conservative, consistent with least-favorable calibration when only a finite contact set binds. LSW exhibits a different issue: under the baseline trimming constant $c_0 = 2^{-9}$, it is undersized in the single-contact case but oversized in smaller samples when two or three contacts bind. Hence a trimming value that calibrates one boundary configuration need not calibrate another.

Under Violated (3), feasible LMW power is lowest and remains below its size-adjusted oracle benchmark. LSW has higher oracle power than LMW, but its feasible rejection rates must be read together with the size distortions in the binding designs. ELR has the highest feasible power and is close to its infeasible benchmark, indicating accurate critical-value estimation by localization and re-centered bootstrap. Because the violation drifts toward the boundary at the $T^{-1/2}$ rate, power changes little with T. Overall, Table 1 shows that ELR has the most accurate binding-size control and the highest feasible power in the baseline local-violation design.

Sensitivity to test parameters. We examine the sensitivity to the subsample exponent b_0 for LMW, the trimming constant c_0 for LSW, and the localization constant d_0 for ELR around their baseline values, using the Binding (3) and Violated (3) designs with $v = (1, 1, 1)'$ and $m_T = \lfloor T^{0.6} \rfloor$. For LMW, larger b_0 raises both size and power. LSW is much more sensitive to trimming: under Binding (3), $c_0 = 2^{-8}$ gives rejection rates of 4.6, 4.1, and 3.4 percent, whereas $c_0 = 2^{-10}$ yields 34.1, 30.9, and 28.9 percent. The corresponding feasible power changes similarly, although infeasible LSW power is unchanged. This confirms that feasible LSW rejection rates are driven partly by trimming-based contact selection, not only by the discriminatory content of the statistic. ELR is stable across $d_0 = 1, 2, 3$: size remains close to 10 percent and power changes little. Complete simulation results are reported in Online Supplement Table 2.

Sensitivity to grid size. We vary the grid exponent m_0 in $m_T = \lfloor T^{m_0} \rfloor$ over $m_0 \in$

SD Inequalities	Test	Param.	$T = 300$	$T = 1000$	$T = 3000$
Slack	Naive		11.2	12.2	12.8
	LMW	$b_0 = 0.7$	0.2	0.2	0.1
	LSW	$c_0 = 2^{-9}$	0.3	0.2	0.2
	ELR	$d_0 = 2$	0.6	0.5	0.5
Binding (1)	Naive		49.4	50.0	49.8
	LMW	$b_0 = 0.7$	5.6	4.7	4.7
	LSW	$c_0 = 2^{-9}$	4.3	4.9	5.3
	ELR	$d_0 = 2$	10.1	10.0	10.0
Binding (2)	Naive		56.5	56.6	56.7
	LMW	$b_0 = 0.7$	8.8	7.7	7.7
	LSW	$c_0 = 2^{-9}$	21.2	12.0	9.7
	ELR	$d_0 = 2$	9.8	9.5	10.1
Binding (3)	Naive		69.5	71.0	71.5
	LMW	$b_0 = 0.7$	8.8	7.3	5.9
	LSW	$c_0 = 2^{-9}$	16.8	14.0	9.6
	ELR	$d_0 = 2$	9.7	9.9	9.9
Violated (3)	Naive		92.9	93.5	93.9
	LMW	$b_0 = 0.7$	25.0	21.3	20.3
	LSW	$c_0 = 2^{-9}$	30.7	29.4	28.7
	ELR	$d_0 = 2$	35.4	38.1	38.6
Infeasible	LMW	$b_0 = 0.7$	30.0	27.9	28.8
	LSW	$c_0 = 2^{-9}$	32.9	31.7	32.7
	ELR	$d_0 = 2$	35.1	37.3	38.9

Table 1: Baseline rejection rates in percent. Slack and Binding panels report empirical size at the nominal 10 percent level; Violated (3) reports feasible power; Infeasible reports size-adjusted oracle power using the simulated Binding (3) null distribution. Baseline constants are $b_0 = 0.7$, $c_0 = 2^{-9}$, $d_0 = 2$, and $m_T = \lfloor T^{0.6} \rfloor$. Results use 5000 MC replications and 1000 resampling replications, with local drift $v = (1, 1, 1)'$.

$0.5, 0.6, 0.7$, holding test-specific parameters fixed. The results do not overturn the baseline conclusions. LMW remains relatively stable across grids but conservative, especially for larger samples. LSW is more sensitive because grid granularity interacts with trimming-based contact selection. ELR maintains size close to the nominal level across grid choices. Its power is somewhat lower for the coarsest grid at $T = 300$ and $T = 1000$, but the difference largely disappears for larger samples and finer grids. This is consistent with localization: the grid must be fine enough to place candidate points near the local minima, but once this occurs, nearby selected minima are highly collinear and span essentially the same local constraint space. Complete simulation results are reported in Online Supplement Table 3.

Drift-vector specification. Table 2 studies how power changes with the direction of the local violation, holding the grid and tuning parameters fixed. Because feasible LSW uses the same baseline trimming constant $c_0 = 2^{-9}$, its power should be interpreted conditional on the size calibration discussed above; the infeasible rows provide the cleaner comparison of directional sensitivity.

Under the parallel drift $v_1 = (1, 1, 1)'$, ELR has the highest feasible and infeasible power, while LSW improves on LMW by aggregating violations across contacts. Under the covariance-balanced vector $v_2 = (0.70, 1.06, 1.25)'$, LSW and ELR are close, especially in the infeasible comparison, showing that covariance balance and ELR favorability are distinct concepts. The largest ELR gains occur under $v_3 = (1.72, 0.73, 0.55)'$: feasible ELR power is 52.9, 59.3, and 61.9 percent for $T = 300, 1000, 3000$, compared with 24.2, 24.3, and 21.2 percent for LMW and 32.6, 32.8, and 30.8 percent for LSW. The infeasible results show the same pattern, so the advantage is not driven by critical-value estimation. This is consistent with the oblique-cone local-power interpretation: ELR is competitive under balanced violations, but its largest gains arise when the violation direction loads strongly on high-contribution rays of the covariance-induced cone.

Drift vector	SD Inequalities	Test	Param.	$T = 300$	$T = 1000$	$T = 3000$
$(1, 1, 1)'$	Violated (3)	LMW	$b_0 = 0.7$	25.0	21.3	20.3
		LSW	$c_0 = 2^{-9}$	30.7	29.4	28.7
		ELR	$d_0 = 2$	35.4	38.1	38.6
	Infeasible	LMW	$b_0 = 0.7$	30.0	27.9	28.8
		LSW	$c_0 = 2^{-9}$	32.9	31.7	32.7
		ELR	$d_0 = 2$	35.1	37.3	38.9
$(0.70, 1.06, 1.25)'$	Violated (3)	LMW	$b_0 = 0.7$	27.6	24.7	23.2
		LSW	$c_0 = 2^{-9}$	32.9	31.0	29.9
		ELR	$d_0 = 2$	31.9	32.5	34.1
	Infeasible	LMW	$b_0 = 0.7$	31.5	30.9	31.5
		LSW	$c_0 = 2^{-9}$	33.7	32.6	33.5
		ELR	$d_0 = 2$	32.0	32.2	34.2
$(1.72, 0.73, 0.55)'$	Violated (3)	LMW	$b_0 = 0.7$	24.2	24.3	21.2
		LSW	$c_0 = 2^{-9}$	32.6	32.8	30.8
		ELR	$d_0 = 2$	52.9	59.3	61.9
	Infeasible	LMW	$b_0 = 0.7$	33.8	34.1	34.1
		LSW	$c_0 = 2^{-9}$	35.9	35.4	36.4
		ELR	$d_0 = 2$	52.2	58.1	62.3

Table 2: Sensitivity of rejection rates to the local violation direction. Entries are feasible and infeasible size-adjusted power in percent for the three-contact violated design. The infeasible rows use the simulated Binding (3) null distribution. The violation directions are normalized to have average component one; all other baseline settings are as in Table 1.

Localization accuracy. We analyze the distribution of the number of candidate local minima selected by the ELR localization rule for the Binding (3) and Violated (3) designs. With the baseline value $d_0 = 2$, the rule selects exactly three candidate minima with high frequency: 94.2, 94.6, and 94.6 percent under Binding (3), and 99.3, 99.2, and 99.3 percent under Violated (3), for $T = 300, 1000, 3000$. Increasing d_0 to 3 essentially eliminates under-selection, while reducing it to 1 increases under-selection. The rule does not produce over-selection in these simulations. Thus the relevant finite-sample issue is occasional under-selection rather than spurious empirical minima, and $d_0 = 2$ provides a practical compromise between retaining the relevant contact set and avoiding unnecessary constraints. Complete simulation results are reported in Online Supplement Table 4.

5 Empirical Application

This section applies the LMW, LSW, and ELR test procedures to monthly returns on ten CBOE SPX option-strategy benchmark indices from June 1988 to June 2026 ($T = 457$), the longest period available at the time of writing. The data are taken from Bloomberg.

BXM, BXY, and BXMD are covered-call strategies that hold the index and write, respectively, an at-the-money call, a 2% out-of-the-money call, and a 30-delta out-of-the-money call. PUT is a cash-secured put-writing strategy, while CMBO combines covered-call and put-writing exposure. PPUT holds the index and buys protective puts, while CLL and CLLZ are collar and put-spread-collar strategies that combine downside protection with written calls. BFLY and CNDR are cash-collateralized volatility-premium strategies based on butterflies and condors, respectively.

For each strategy, we apply each of the three procedures to test dominance by each of the nine alternatives at the 10% level and count the rejections. Since the strategies trade off upside participation, option-premium income, downside protection, and exposure to large market moves, few true dominance relations are expected a priori. Higher rejection counts therefore indicate greater ability to rule out economically implausible dominance relations.

Implementation follows Sections 2.3 and 4.2, including robustness checks for grid size and test parameters. To account for scale dependence of the calibration, we rescale returns to match the standard deviation $\sigma_Y = 0.2$ in the experiment; this common positive transformation does not affect SD relations. Although the data are not necessarily IID, monthly S&P 500-based index returns are less exposed to the market-microstructure dependence typical of high-frequency or illiquid-stock returns. Any remaining serial dependence is likely to affect all three procedures similarly, so relative rejection frequencies should be more robust than individual p-values.

Table 3 summarizes the results. The table shows a substantially larger number of rejections for ELR than for LMW and LSW, consistent with the power gains documented in the simulations. The most striking result concerns BFLY. Under the baseline specification, LMW and LSW do not reject the null that BFLY is dominated by any other strategy, whereas ELR rejects it in seven out of nine cases. This appears related to BFLY's Treasury-bill core and capped option losses: reversing its tail advantage relative to SPX-based alternatives would require substantial empirical-likelihood reweighting of sparse left-tail observations. Thus, although the empirical tail gap is noisy, ELR is less affected than LMW and LSW by pointwise tail noise in this comparison.

References

Andrews, D.W.K., Barwick, P.J., 2012. Inference for parameters defined by moment inequalities: A recommended moment selection procedure. Econometrica 80, 2805–2826.

Andrews, D.W.K., Soares, G., 2010. Inference for parameters defined by moment inequalities using generalized moment selection. Econometrica 78, 119–157.

Arvanitis, S., Hallam, M., Post, T., Topaloglou, N., 2019. Stochastic spanning. Journal of Business & Economic Statistics 37, 573–585. doi:10.1080/07350015.2017.1391099.

Arvanitis, S., Post, T., 2023. Stochastic arbitrage opportunities. Management Science doi:10.1287/mnsc.2022.4584.

Chen, X., Tabri, K., 2019. Jackknife empirical likelihood for inequality constraints. Journal of Econometrics 210, 1–25.

Davidson, R., Duclos, J., 2013. Testing for restricted stochastic dominance. Econometric Reviews 32, 84–125. doi:10.1080/07474938.2012.690332.

Test	Grid	Param.	BXM	BXY	BXMD	PUT	CMBO	PPUT	CLL	CLLZ	BFLY	CNDR	Total
LMW	$T^{0.6}$	$b_0 = 0.7$	8	8	8	9	8	2	4	5	0	9	61
	$T^{0.6}$	$b_0 = 0.6$	8	8	8	9	8	1	4	4	0	9	59
	$T^{0.6}$	$b_0 = 0.8$	8	8	8	9	8	2	6	5	0	9	63
	$T^{0.5}$	$b_0 = 0.7$	8	8	7	9	8	1	4	5	0	9	59
	$T^{0.7}$	$b_0 = 0.7$	8	8	8	9	8	2	6	4	0	9	62
LSW	$T^{0.6}$	$c_0 = 2^{-9}$	7	5	4	9	6	0	2	3	0	8	44
	$T^{0.6}$	$c_0 = 2^{-10}$	7	5	4	9	6	0	2	3	0	8	44
	$T^{0.6}$	$c_0 = 2^{-8}$	7	5	4	9	6	0	3	3	2	8	47
	$T^{0.5}$	$c_0 = 2^{-9}$	7	5	4	8	6	1	2	3	0	8	47
	$T^{0.7}$	$c_0 = 2^{-9}$	7	5	6	9	6	0	2	3	1	9	47
ELR	$T^{0.6}$	$d_0 = 2$	8	8	7	9	8	4	7	4	7	9	71
	$T^{0.6}$	$d_0 = 1$	8	8	7	9	8	6	7	5	7	9	74
	$T^{0.6}$	$d_0 = 3$	8	8	7	9	8	4	7	4	7	9	71
	$T^{0.5}$	$d_0 = 2$	8	8	7	9	8	4	7	4	7	9	71
	$T^{0.7}$	$d_0 = 2$	8	8	7	9	7	4	7	4	7	9	70

Table 3: Pairwise SD rejection counts for the CBOE benchmark strategies. For each evaluated strategy, the table reports the number of pairwise tests, out of nine comparisons, that reject the null that an alternative strategy dominates the evaluated strategy at the 10% significance level.

Kitamura, Y., 2006. Empirical likelihood methods in econometrics: Theory and practice. Econometric Theory 22, 342–381.

Levy, H., 2016. Stochastic Dominance: Investment Decision Making under Uncertainty. 3 ed., Springer International Publishing, Cham.

Linton, O., Maasoumi, E., Whang, Y.J., 2005. Consistent testing for stochastic dominance under general sampling schemes. The Review of Economic Studies 72, 735–765.

Linton, O., Song, K., Whang, Y.J., 2010. An improved bootstrap test of stochastic dominance. Journal of Econometrics 154, 186–202.

Owen, A.B., 1988. Empirical likelihood ratio confidence intervals for a single functional. Biometrika 75, 237–249.

Perrakis, S., 2019. Stochastic Dominance Option Pricing: An Alternative Approach to Option Market Research. Springer International Publishing, Cham, Switzerland. doi:10.1007/978-3-030-11590-6.

Post, T., 2017. Empirical tests for stochastic dominance optimality. Review of Finance 21, 793–810. doi:10.1093/rof/rfw010.

Post, T., Potì, V., 2017. Portfolio analysis using stochastic dominance, relative entropy, and empirical likelihood. Management Science 63, 153–165. doi:10.1287/mnsc.2015.2325.

Whang, Y.J., 2019. Econometric analysis of stochastic dominance: Concepts, methods, tools, and applications. Cambridge University Press.

Supplemental Material for: Empirical Likelihood Tests for Pairwise Stochastic Dominance

Stelios Arvanitis[*], Richard McGee[†], and Thierry Post[‡]

July 8, 2026

Abstract

This Supplement contains details and proofs regarding the statistical theory established in the Main Text, as well as additional simulation design details and sensitivity analysis covering the test parameters, grid size, and localization accuracy.

Contents

[*]Athens University of Economics and Business, Greece. Email: stelios@aueb.gr

[†]University College Dublin, Ireland. Email: richard.mcgee@ucd.ie

[‡]Graduate School of Business of Nazarbayev University, Kazakhstan. E-mail: thierrypost@hotmail.com.
Funding from Nazarbayev University is acknowledged under the Faculty Development Competitive Research Grants Program (No. 201223FD8832) and Research Matching Grant Program (No. 110326MRP0303).

1 Statistical Theory

This section develops the asymptotic theory for the testing procedures considered in this study. Section 1.1 sets out the probabilistic and analytical framework for the underlying processes and the gap function, and provides a detailed statement and discussion of Assumption 3.1 in the main text. We then establish first-order properties—exactness, conservativeness, and consistency—of the procedures under the null and under fixed alternatives. This clarifies when different calibration schemes yield valid inference and when size distortions arise due to incorrect treatment of binding constraints. These results–derived in the current Section 1.2–constitute Theorem 3.1 in the main text. We finally turn to local (Pitman) asymptotics to study finer power differences among tests that are already first-order valid. The analysis draws on the properties of the covariance structure and the contact set. These results derived in the present Sections 1.3 and 1.4 here constitute Theorem 3.3 as well as Corollaries 3.1-3.3 in the main text, and shed light in the Geometric Interpretation and Comparison section in the main text. All proofs and auxiliary results are put in the Appendix of the current Supplement. In what follows $\rightsquigarrow$ denotes convergence in distribution.

1.1 Probabilistic and regularity assumptions

We collect and discuss the probabilistic and regularity conditions used throughout the asymptotic analysis.

Assumption 1.1 (Stationarity and absolute regularity)**.** *The process $\{(X_t, Y_t)\}_{t\in\mathbb{Z}}$ is strictly stationary and absolutely regular (β-mixing) with coefficients $\beta(k)$ satisfying $\beta(k) \le C\, k^{-(1+\epsilon)}$ ($k \ge 1$) for some constants $C < \infty$ and $\epsilon > 0$.*

Assumption 1.1 is satisfied by a broad class of models commonly used in financial and economic applications, including geometrically ergodic Markov processes (such as standard stochastic volatility and GARCH models under usual conditions), finite–state hidden Markov models, and stable linear processes with weakly dependent innovations. These classes often exhibit exponential or polynomial β–mixing and therefore satisfy Assumption 1.1 as a fortiori. The assumption is strong enough to support uniform LLNs and functional CLTs for the Lipschitz moment class $\{g_z(\cdot) : z \in \mathcal{Z}\}$ employed in the SSD tests.

Assumption 1.2 (Moment and integrability conditions). *There exists $\delta \geq 1, C^\star > 0$ such that*

$$\mathbb{E}[|X_t|^{2+\delta}] + \mathbb{E}[|Y_t|^{2+\delta}] \leq C^\star.$$

Furthermore, $\epsilon > 2 + \frac{4}{\delta}$.

This assumption along with the uniform Lipschitz properties of g_z ensures that all moment functions are square-integrable and that the long-run covariance matrix Σ in Equation 4 in the main text is well-defined and finite. Assumptions 1.1-1.2 imply the applicability of a functional CLT for the empirical process constructed by Δ_T–see Theorem 4, along with the Application 4 (Condition 2.15) of Theorem 1 of Doukhan et al. (1995).

Assumption 1.3 (Finite strict–local minima set). *The finite set of strict local minima of Δ on $\mathcal{Z}$, for which $\Delta \leq 0$, is denoted by $\mathcal{C}_{\ell,f} = \{c_1^\star, \ldots, c_{J_{\ell,f}}^\star\} \subset \mathcal{Z}$. Also, for each j there exist $r_j > 0$ and $\kappa_j > 0$ such that on the neighborhood $N_j := (c_j^\star - r_j, c_j^\star + r_j) \cap \mathcal{Z}$,*

$$\Delta(z) - \Delta(c_j^\star) \geq \kappa_j (z - c_j^\star)^2, \qquad z \in N_j. \tag{1}$$

When the mean restriction is imposed, the possible contact or violation at ∞ is handled separately through $\Delta(\infty)$ and g_∞. Under the null hypothesis, the full contact set is $C = C_f \cup C_\infty$, and $J = |C|$. If $J > 0$, Σ is positive definite.

Under the null hypothesis, since $\Delta(z) \geq 0$ for all $z \in \mathcal{Z}_\infty$, every finite element of $\mathcal{C}_{\ell,f}$ satisfies $\Delta(c_j^\star) = 0$. Hence $\mathcal{C}_{\ell,f}$ coincides with the finite component C_f of the non-trivial contact set. If the mean restriction is imposed and $\Delta(\infty) = 0$, then $C_\infty = \{\infty\}$ is added to the contact set; otherwise $C_\infty = \emptyset$. Under fixed alternatives, $\mathcal{C}_{\ell,f}$ must contain at least one strict local minimum with $\Delta(c_j^\star) < 0$, or the mean restriction must satisfy $\Delta(\infty) < 0$, corresponding to genuine violations of the dominance inequalities. Thus (1) is a local quadratic-separation condition around relevant finite minima, rather than a boundary-null restriction.

The condition $J < \infty$ is generic in smooth models, as discussed in Section 2.2 in the main text. For finite contacts, when Δ is twice continuously differentiable, then the local strong convexity requirement in (1) follows by strict positivity of the Hessian at each respective local minimum. Definiteness of Σ under the null follows by algebraic linear independence of the set of moment functions that comprise the binding inequalities because Σ is a Gram matrix.

Assumption 1.4 (Grid approximation on expanding compacts)**.** *There exists a deterministic sequence $R_T \uparrow \infty$ such that:*

*(i) (*PK convergence on compacts*)*

$$\mathcal{Z}_T \cap [-R_T, R_T] \xrightarrow{p} \mathcal{Z} \cap [-R_T, R_T]$$

in the Painlevé–Kuratowski (PK) topology;

*(ii) (*Local density around finite contacts*) writing $C_f = \{c_{f,1}, \ldots, c_{f,J_f}\}$, for each $j = 1, \ldots, J_f$,*

$$\mathrm{dist}(c_{f,j}, \mathcal{Z}_T) := \inf_{z \in \mathcal{Z}_T} |z - c_{f,j}| \xrightarrow{p} 0.$$

Assumption 1.4 is mild and is satisfied by essentially any threshold grid that becomes dense on expanding compacts. For example, if $\mathcal{Z}_T$ is constructed from the sample (e.g. quantile grids, grids restricted to observed support, or grids obtained after trimming extreme values) and satisfies, w.h.p., a maximal gap bound $\sup\{|z - z'| : \ z, z' \text{ adjacent in } \mathcal{Z}_T \cap [-R_T, R_T]\} \le h_T$ with $h_T \downarrow 0$, then $\mathcal{Z}_T \cap [-R_T, R_T] \xrightarrow{p} \mathcal{Z} \cap [-R_T, R_T]$ in the PK sense and (ii) follows provided each finite contact $c_{f,j}$ lies in the interior of $\mathcal{Z}$.

1.2 Limit theory: null, Pitman drifts, fixed alternatives

This section collects the first-order weak limits of the three statistics introduced in Section 2.3. Given the hypotheses structure, we consider local (Pitman) alternatives of the form

$$\Delta_T^{(h)}(z) = \Delta(z) + T^{-1/2} h(z), \quad z \in \mathcal{Z}_\infty, \tag{2}$$

where $h : \mathcal{Z}_\infty \to \mathbb{R}$ is a deterministic drift function. This covers the canonical $\sqrt{T}$-local departures from the boundary of H_0. For fixed alternatives, it is assumed that $\inf_{z \in \mathcal{Z}_\infty} \Delta(z) < 0$.

1.2.1 Limit theory for the three statistics

Theorem 1.1 (Limit theory for LMW)**.** *Suppose Assumptions 1.1-1.4 and let $\mathbb{G}$ denote a tight mean-zero Gaussian process with covariance induced by the long-run covariance kernel of $\{g_z(X_t, Y_t)\}$. Then,* *(i)* Null. *Under* $\mathbf{H}_0$,

$$\mathrm{LMW}_T \rightsquigarrow \sup_{z\in C}\big[-\mathbb{G}(z)\big]. \tag{3}$$

(ii) Pitman drifts. *Under* (2)*, and if Assumptions 1.1-1.2 hold over a weak topology open neighborhood of* $\mathbb{P}$*, with uniform constants* $C, C^\star, \delta, \epsilon$*, then*

$$\mathrm{LMW}_T \rightsquigarrow \sup_{z\in C}\big[-\{\mathbb{G}(z)+h(z)\}\big]. \tag{4}$$

(iii) Fixed alternatives. *If* $\inf_{z\in\mathcal{Z}_\infty}\Delta(z)<0$*, and for* $J\geq 0$*, then* $LMW_T\to\infty$ *in probability.*

(iv) Degenerate-contact case. *If* $J=0$*, then under the* $\mathbf{H}_0$, $\mathrm{LMW}_T \rightsquigarrow 0$.

Theorem 1.2 (Limit theory for LSW)**.** *Suppose Assumptions 1.1-1.4 and let* $\mathbb{G}$ *denote the Gaussian process introduced above. Suppose that* $\nu_T \rightsquigarrow \nu$ *a tight measure on* $\mathcal{Z}_\infty$*, that puts positive mass on* C*.*

(i) Null. *Under* $\mathbf{H}_0$,

$$\mathrm{LSW}_T \rightsquigarrow \int_C \big[-\mathbb{G}(z)\big]_+^2\,\nu(dz). \tag{5}$$

(ii) Pitman drifts. *Under* (2)*, and if Assumptions 1.1-1.2 hold over a weak open neighborhood of* $\mathbb{P}$*, with uniform constants* $C, C^\star, \delta, \epsilon$*, then*

$$\mathrm{LSW}_T \rightsquigarrow \int_C \big[-\{\mathbb{G}(z)+h(z)\}\big]_+^2\,\nu(dz). \tag{6}$$

(iii) Fixed alternatives. *If* $\inf_{z\in\mathcal{Z}_\infty}\Delta(z)<0$*, then for* $J\geq 0$*,* $LSW_T\to\infty$ *in probability.*

(iv) Degenerate contact case. *If* $J=0$*, then under the* $\mathbf{H}_0$, $\mathrm{LSW}_T \rightsquigarrow 0$.

Theorem 1.3 (Limit theory for localized ELR)**.** *Suppose Assumptions 1.1–1.4 and that* $\ell_T\to\infty$*,* $\ell_T T^{1/(2+\delta)-1/2}\to 0$*. Then,*

(i) Null. *Under* $\mathbf{H}_0$*,* $\widehat{C}_T \xrightarrow{p} C$ *in the PK topology, and*

$$\mathrm{ELR}_T \rightsquigarrow Q(\Sigma) := \inf_{\eta\in\mathbb{R}_+^J}\,(W-\eta)^\top\Sigma^{-1}(W-\eta), \tag{7}$$

where $W\sim N(0,\Sigma)$ *and* $\mathbb{R}_+^J$ *is the nonnegative orthant. Equivalently,* ELR_T *converges to a* $\bar{\chi}_J^2$ *distribution with weights determined by* Σ*.*

(ii) Pitman drifts. *Under* (2) *with drift function* h*, and if Assumptions 1.1–1.2 hold over a weak open neighborhood of* $\mathbb{P}$*, with uniform constants* $C, C^\star, \delta, \epsilon$*, we again have the shifted*

projection representation

$$\mathrm{ELR}_T \;\rightsquigarrow\; \inf_{\eta\in\mathbb{R}_+^J} (W+\mu_h-\eta)^\top\Sigma^{-1}(W+\mu_h-\eta), \tag{8}$$

where $\mu_h := (h(z))_{z\in C}$ denotes the drift vector on the population contact coordinates.

(iii) Fixed alternatives. *If $\exists z_0 \in \mathcal{Z}_\infty$ such that $\Delta(z_0) < 0$, then $ELR_T \to \infty$ in probability.*

(iv) Degenerate-contact case. *If $J = 0$, then under $\mathbf{H}_0$, $\mathrm{ELR}_T \rightsquigarrow 0$.*

The strengthening of Assumptions 1.1-1.2 to hold locally uniformly around $\mathbb{P}$ with uniform constants facilitates the use of locally uniform versions of the limit theorems employed under the null; they typically hold for interior versions of standard stationary econometric time series models.

The preceding results show that, under weak dependence and smooth contact geometry, the ELR, LMW, and LSW statistics all admit well-defined weak limits driven by the same Gaussian process restricted to the population contact set. Differences across procedures arise from how this limiting object is mapped into a scalar statistic: ELR exploits the full multivariate cone geometry through a self-normalized quadratic form, LMW collapses contact information via an extremal functional, and LSW aggregates violations through an L^2-type integral. These distinctions determine the appropriate calibration, exactness and conservativeness properties under the null, and consistency under fixed and local alternatives, and provide the basis for the Pitman efficiency comparisons developed in what follows.

1.2.2 Critical values, exactness, conservativeness, consistency

The following results describe the first order properties of the testing procedures examined as $T \to \infty$. Those are based on the limiting theories of the statistics established above, as well as on the asymptotic properties of their respective rejection regions. We obtain the following:

Proposition 1.1 (LMW critical values and test properties)**.** *Let $\psi_\alpha^{\mathrm{SS}}$ be the LMW test rejecting when $\mathrm{LMW}_T > \hat{q}_{1-\alpha}^{\mathrm{SS}}$ (subsampling critical value). Assume that Assumptions 1.1-1.3 hold. Then:*

(i) Subsampling critical value. *Suppose $\mathbf{H}_0$ holds. If $J > 0$ then the subsampling distribution of $\mathrm{LMW}_{t,b}$ consistently estimates the law of the limit in (3) provided $b \to \infty$ and $b/T \to 0$. Hence $\hat{q}_{1-\alpha}^{\mathrm{SS}} \to_p q_{1-\alpha}$, the $(1-\alpha)$ quantile of the LMW limit. Thereby, $\psi_\alpha^{\mathrm{SS}}$ is asymptotically exact. If $J = 0$ then the test is asymptotically conservative.*

(ii) Consistency. *Under fixed alternatives, $\mathrm{LMW}_T \to \infty$ and the subsampling procedure is consistent.*

Proposition 1.2 (LSW bootstrap critical values and test properties)**.** *Let $q^*_{1-\alpha,T}(c)$ be the conditional $(1-\alpha)$-quantile of LSW^*_T, where the bootstrap pseudo-sample is generated either by the ordinary nonparametric bootstrap under independence or by a block bootstrap under dependence with block length $b_T \to \infty$, $b_T/T \to 0$. Suppose Assumptions 1.1–1.4 hold, and suppose the trimming sequence satisfies $c_T \to 0$ and $\sqrt{T}c_T \to \infty$. Assume also that the trimming rule is asymptotically correct, i.e. $\mathbb{P}\{J_T = J_C\} \to 1$, where $J_C = \{j : z_{T,j} \to C\}$ denotes the index set corresponding to the population contact set. Then:*

(i) Under $\mathbf{H}_0$, conditionally on the data,

$$\mathrm{LSW}^*_T \rightsquigarrow_p \int_C [-\mathbb{G}(z)]^2_+ \,\nu(dz).$$

Consequently, $q^*_{1-\alpha,T}(c) \xrightarrow{p} q_{1-\alpha}$, where $q_{1-\alpha}$ is the $(1-\alpha)$-quantile of the LSW limit.

(ii) If $J \geq 1$, the feasible LSW test is asymptotically exact:

$$\mathbb{P}(\mathrm{LSW}_T > q^*_{1-\alpha,T}(c)) \to \alpha.$$

If $J = 0$, then $\mathrm{LSW}_T \rightsquigarrow 0$ and the test is asymptotically conservative.

(iii) Under fixed alternatives satisfying $\inf_{z\in\mathcal{Z}_\infty} \Delta(z) < 0$, $\mathrm{LSW}_T \to \infty$ in probability, while $q^*_{1-\alpha,T}(c) = O_p(1)$. Hence the test is consistent.

Proposition 1.3 (Localized bootstrap ELR critical values and test properties)**.** *Suppose Assumptions 1.1–1.4 hold, with $\delta \geq 1$. Let the EL block length ℓ_T and the bootstrap resampling block length b_T satisfy*

$$\ell_T \to \infty, \qquad \ell_T T^{1/(2+\delta)-1/2} \to 0,$$

and

$$b_T \to \infty, \qquad b_T/T \to 0, \qquad \ell_T/b_T \to 0.$$

Assume that the bootstrap is a moving-block bootstrap, or another dependence-preserving block bootstrap satisfying the usual conditional CLT for absolutely regular sequences. Then the following statements hold. (i) Bootstrap critical values under $\mathbf{H}_0$, exact-contact case. *If $J \geq 1$, then under $\mathbf{H}_0$,*

$$\widetilde{c}^*_{\alpha,T} \xrightarrow{p} c_\alpha(\Sigma),$$

where $c_\alpha(\Sigma)$ is the $(1-\alpha)$-quantile of the distribution of $Q(\Sigma)$. Consequently,

$$\mathbb{P}\big(\mathrm{ELR}_T > \widetilde{c}^*_{\alpha,T}\big) \to \alpha.$$

(ii) Degenerate-contact case. *If $J=0$, then under $\mathbf{H}_0$, $\mathbb{P}(\phi^*_\alpha = 1) \to 0$.* *(iii)* Fixed alternatives. *If $\inf_{z \in \mathcal{Z}_\infty} \Delta(z) < 0$, then $\mathrm{ELR}_T \to \infty$ in probability, whereas the recentered bootstrap critical values remain bounded in probability: $\widetilde{c}^*_{\alpha,T} = O_p(1)$. Hence $\mathbb{P}(\phi^*_\alpha = 1) \to 1$.*

This subsection established the first-order operating characteristics of the ELR, LMW, and LSW tests, combining their weak limit theories with the asymptotic behavior of the corresponding critical value procedures. When the contact set is nonempty ($J \geq 1$), each test can be calibrated to achieve asymptotic exactness under the null, while all procedures are conservative in the strictly interior case ($J = 0$). Under fixed alternatives, all three statistics diverge and yield consistent tests, whereas under $\sqrt{T}$-Pitman drifts their local power is governed by distinct functionals of the same Gaussian limit on the contact set. These results provide a unified foundation for comparing the tests' efficiency and robustness, which is pursued in the subsequent Pitman drift analysis.

1.3 Pitman drifts and local power expansions

This subsection develops a local asymptotic power analysis for the three dominance tests based directly on derivatives of the limiting rejection probability under Gaussian shift alternatives. We work with the Taylor expansion of the rejection probability around the null and compare competing tests lexicographically. The framework is extendable to higher-order terms.

1.3.1 Contact-reduced Gaussian shift experiment

For the contact set $C = \{c_1, \ldots, c_J\}$ define the contact-reduced empirical process

$$\hat{\mathbf{g}}_T := \sqrt{T}\,\hat{\Delta}_T(C) = \sqrt{T}\,\big(\hat{\Delta}_T(c_1), \ldots, \hat{\Delta}_T(c_J)\big)^\top.$$

Under $\mathbf{H}_0$, and given our assumption framework, the previous results showed that the contact-restricted central limit theorem holds:

$$\hat{\mathbf{g}}_T \;\rightsquigarrow\; W, \qquad W \sim N(0, \Sigma), \tag{9}$$

for the positive definite covariance matrix $\Sigma \in \mathbb{R}^{J \times J}$.

Local alternatives are indexed by a deterministic drift direction h through the contact-reduced mean vector $\mu_h := \big(h(c_1), \ldots, h(c_J)\big)^\top$, with $h(c_j) \leq 0$ with strict inequality for at least one j, and the Pitman sequence

$$\mathbf{H}_{T,h}: \quad \Delta(C) = \frac{1}{\sqrt{T}}\,\mu_h. \tag{10}$$

Our previous results based on enhancements of the probabilistic properties of the processes involved in a weak neighborhood of the null implied that under the distributions that inhabit the Pitman sequence, (9) strengthens to the Gaussian shift experiment

$$\hat{\mathbf{g}}_T \rightsquigarrow W + \mu_h, \qquad W \sim N(0, \Sigma). \tag{11}$$

Thereby, and for a given scalar parameter t that is conveniently close to zero, local power comparisons can be conducted in the limiting experiment $W_t := W + t\mu_h$.

1.3.2 Generic local power expansion for Gaussian-shift statistics

Let $\Psi : \mathbb{R}^J \to \mathbb{R}$ be a measurable (limiting) test functional and define

$$T_t := \Psi(W + t\mu_h), \qquad T_0 = \Psi(W).$$

Let c_α denote the $(1-\alpha)$ quantile of T_0 under $\mathbf{H}_0$. The limiting rejection probability under drift $t\mu_h$ is

$$\pi(t; h) := \mathbb{P}(\Psi(W + t\mu_h) > c_\alpha)\,. \tag{12}$$

Define the fixed rejection region

$$\mathcal{R} := \{w \in \mathbb{R}^J : \Psi(w) > c_\alpha\}.$$

Then

$$\pi(t; h) = \int_{\mathcal{R}} \varphi_\Sigma(w - t\mu_h)\, dw,$$

where φ_Σ is the $N(0, \Sigma)$ density.

Differentiation under Gaussian shift. The Gaussian score identities yield

$$\nabla \varphi_\Sigma(w) = -\varphi_\Sigma(w)\Sigma^{-1}w, \qquad \nabla^2 \varphi_\Sigma(w) = \varphi_\Sigma(w)\big(\Sigma^{-1}ww^\top\Sigma^{-1} - \Sigma^{-1}\big).$$

Using those, along with some regularity properties for the boundary of the limiting rejection region, we obtain-in what follows $\mathcal{H}_{J-1}$ denotes the $J-1$ dimensional Hausdorff measure:

Lemma 1.1 (Gaussian-shift differentiation and boundary (Stein) representations)**.** *Assume that c_α is such that $\mathbb{P}(\Psi(W) = c_\alpha) = 0$, and that $\mathcal{R}$ is an open set with Lipschitz boundary $\partial\mathcal{R}$ and outward unit normal $n(\cdot)$ defined $\mathcal{H}_{J-1}$-a.e. on $\partial\mathcal{R}$. Assume moreover that the Gaussian surface integrals appearing below are finite. Then, π is twice differentiable at $t = 0$ and admits* *the expansion*

$$\pi(t;h) = \pi(0;h) + t\,\pi'(0;h) + \frac{t^2}{2}\pi''(0;h) + o(t^2), \qquad t \downarrow 0,$$

with the following equivalent representations.

(i) Volume (score/Hessian) forms. *Writing $\pi(0;h) = \mathbb{P}(W \in \mathcal{R})$, we have*

$$\pi'(0;h) = \int_{\mathcal{R}} \mu_h^\top \nabla \varphi_\Sigma(w)\,dw = \mathbb{E}\big[\mu_h^\top \Sigma^{-1} W\,\mathbf{1}\{W \in \mathcal{R}\}\big]\,, \tag{13}$$

$$\begin{aligned}\pi''(0;h) &= \int_{\mathcal{R}} \mu_h^\top \nabla^2 \varphi_\Sigma(w) \mu_h\,dw \\ &= \mathbb{E}\Big[\big(\mu_h^\top \Sigma^{-1} W\big)^2\,\mathbf{1}\{W \in \mathcal{R}\}\Big] - \big(\mu_h^\top \Sigma^{-1}\mu_h\big)\mathbb{P}(W \in \mathcal{R}).\end{aligned} \tag{14}$$

(ii) Boundary (generalized Stein / divergence) forms. *We also have the surface-integral representations*

$$\pi'(0;h) = -\int_{\partial\mathcal{R}} (\mu_h^\top n(w))\,\varphi_\Sigma(w)\,d\mathcal{H}_{J-1}(w), \tag{15}$$

$$\begin{aligned}\pi''(0;h) &= \int_{\partial\mathcal{R}} n(w)^\top\big(\mu\mu_h^\top \nabla\varphi_\Sigma(w)\big)\,d\mathcal{H}_{J-1}(w) \\ &= \int_{\partial\mathcal{R}} (\mu_h^\top n(w))\big(\mu_h^\top \nabla\varphi_\Sigma(w)\big)\,d\mathcal{H}_{J-1}(w) \\ &= -\int_{\partial\mathcal{R}} (\mu_h^\top n(w))\big(\mu_h^\top \Sigma^{-1} w\big)\,\varphi_\Sigma(w)\,d\mathcal{H}_{J-1}(w).\end{aligned} \tag{16}$$

1.3.3 Lexicographic comparison of local power

Let two tests A and B adhere to the previous and thus have local power expansions

$$\pi_A(t;h) = \alpha + t\,\pi_A^{(1)}(0;h) + \frac{t^2}{2}\,\pi_A^{(2)}(0;h) + o(t^2),$$

$$\pi_B(t;h) = \alpha + t\,\pi_B^{(1)}(0;h) + \frac{t^2}{2}\,\pi_B^{(2)}(0;h) + o(t^2).$$

We say that test A is locally more powerful than B in direction h if

$$\big(\pi_A^{(1)}(0;h), \pi_A^{(2)}(0;h), \dots\big) \succ_{\text{lex}} \big(\pi_B^{(1)}(0;h), \pi_B^{(2)}(0;h), \dots\big),$$

i.e. the first nonzero derivative of $\pi_A(t;h) - \pi_B(t;h)$ at $t = 0$ is positive. This ordering is directly extendable to higher-order terms whenever lower-order derivatives coincide.

1.3.4 Application of generalized Stein formulas to the competing tests

We now apply the boundary (generalized Stein) representations derived in Lemma 1.1 to the limiting rejection regions of the three competing dominance tests. For each test, we characterize explicitly the geometry of the rejection region $\mathcal{R}$, its boundary $\partial\mathcal{R}$, the outward normal vector $n(\cdot)$, and the resulting first- and second-order derivatives $\pi'(0;h)$ and $\pi''(0;h)$ under Pitman drifts. This yields test-specific local power expansions that can be compared lexicographically. The Lipschitz-type regularity conditions about the boundary of the rejection region as well as the existence of the outward normal vector also follow easily from the analyses below.

1.3.5 Application to the LMW test

We begin by applying the general Gaussian–shift and boundary–Stein representations of Lemma 1.1 to the Kolmogorov–Smirnov / LMW–type test. This statistic targets the most severe local violation among the binding constraints and corresponds to a supremum functional of the contact–reduced Gaussian vector.

Limiting functional and rejection region. The LMW functional is

$$\Psi_{\mathrm{LMW}}(W) = \sup_{1\le j\le J}(-W_j) = -\inf_{1\le j\le J} W_j.$$

Let $c_{\mathrm{LMW}} > 0$ denote the $(1-\alpha)$ critical value of $\Psi_{\mathrm{LMW}}(W)$ under $W \sim N(0,\Sigma)$. The limiting rejection region is therefore

$$\mathcal{R}_{\mathrm{LMW}} = \left\{w \in \mathbb{R}^J : \min_{1\le j\le J} w_j < -c_{\mathrm{LMW}}\right\}. \tag{17}$$

Boundary decomposition. The boundary $\partial\mathcal{R}_{\mathrm{LMW}}$ is the union of J $(J-1)$–dimensional faces,

$$\partial\mathcal{R}_{\mathrm{LMW}} = \bigcup_{j=1}^{J} \partial\mathcal{R}^{(j)}_{\mathrm{LMW}}, \qquad \partial\mathcal{R}^{(j)}_{\mathrm{LMW}} = \Big\{w : \ w_j = -c_{\mathrm{LMW}}, \ \ w_k \ge -c_{\mathrm{LMW}} \ \forall k \ne j\Big\},$$

up to a $\mathcal{H}_{J-1}$ null set that represents that cases of ties in more than one set of coordinates in the optimization above. At $\mathcal{H}_{J-1}$–a.e. point of $\partial\mathcal{R}^{(j)}_{\mathrm{LMW}}$, the outward unit normal vector is $n^{(j)} = e_j$, reflecting that the rejection region extends in the direction of decreasing w_j.

First derivative of local power. Applying the boundary representation (15) yields

$$\pi'_{\mathrm{LMW}}(0;h) = -\int_{\partial\mathcal{R}_{\mathrm{LMW}}} (\mu_h^\top n(w))\,\varphi_\Sigma(w)\,d\mathcal{H}_{J-1}(w)$$
$$= -\sum_{j=1}^{J} \mu_{h,j} \int_{\partial\mathcal{R}^{(j)}_{\mathrm{LMW}}} \varphi_\Sigma(w)\,d\mathcal{H}_{J-1}(w). \tag{18}$$

Since $\mu_{h,j} \le 0$ for all j, with strict inequality for at least one binding contact, each term in (18) is nonnegative and the derivative is strictly positive whenever the drift enters the alternative along at least one coordinate.

Second derivative of local power. Similarly, the second derivative follows from (16):

$$\pi''_{\mathrm{LMW}}(0;h) = -\sum_{j=1}^{J} \int_{\partial\mathcal{R}^{(j)}_{\mathrm{LMW}}} (\mu_h^\top n^{(j)})\big(\mu_h^\top \Sigma^{-1} w\big)\,\varphi_\Sigma(w)\,d\mathcal{H}_{J-1}(w)$$
$$= -\sum_{j=1}^{J} \mu_{h,j} \int_{\partial\mathcal{R}^{(j)}_{\mathrm{LMW}}} \big(\mu_h^\top \Sigma^{-1} w\big)\,\varphi_\Sigma(w)\,d\mathcal{H}_{J-1}(w), \tag{19}$$

which captures curvature effects of the Gaussian density along the coordinatewise faces of the rejection region.

The LMW test reacts to local alternatives through a union of coordinatewise half–spaces. Its first–order local power is therefore driven by a weighted sum of negative drift components, each weighted by the Gaussian surface mass of the corresponding boundary face. This geometry explains why LMW is particularly sensitive to sparse local violations concentrated on a unique binding contact.

1.3.6 Application to the LSW test

We now apply the Gaussian–shift differentiation and boundary representations of Lemma 1.1 to the LSW test. Unlike LMW, which is driven by an extremal coordinate, the LSW statistic aggregates local violations across binding contacts through a second order polynomial, inducing a smooth and curved rejection boundary.

Limiting functional and rejection region. The contact–reduced LSW limiting functional is

$$\Psi_{\mathrm{LSW}}(W) = \sum_{j=1}^{J} a_j\,[-W_j]_+^2, \qquad a_j > 0,$$

where $\{a_j\}_{j=1}^J$ are deterministic positive weights induced by the limiting measure ν on the contact set. Let $c_{\text{LSW}} > 0$ denote the $(1-\alpha)$ critical value of $\Psi_{\text{LSW}}(W)$ under $W \sim N(0, \Sigma)$. The limiting rejection region is therefore

$$\mathcal{R}_{\text{LSW}} = \Big\{ w \in \mathbb{R}^J : \sum_{j=1}^J a_j \, [-w_j]_+^2 > c_{\text{LSW}} \Big\}. \tag{20}$$

Boundary and outward normal. The boundary $\partial\mathcal{R}_{\text{LSW}}$ is the $(J-1)$–dimensional level set

$$\partial\mathcal{R}_{\text{LSW}} = \Big\{ w : \sum_{j=1}^J a_j \, [-w_j]_+^2 = c_{\text{LSW}} \Big\}.$$

It admits a natural decomposition according to the set of active (negative) coordinates. For any nonempty index set $S \subset \{1, \ldots, J\}$ define

$$\partial\mathcal{R}_{\text{LSW}}(S) := \Big\{ w \in \mathbb{R}^J : w_j < 0 \text{ for } j \in S, \quad w_j \geq 0 \text{ for } j \notin S, \quad \sum_{j \in S} a_j w_j^2 = c_{\text{LSW}} \Big\}.$$

Then the boundary decomposes as the disjoint union

$$\partial\mathcal{R}_{\text{LSW}} = \bigcup_{\emptyset \neq S \subset \{1,\ldots,J\}} \partial\mathcal{R}_{\text{LSW}}(S),$$

up to $\mathcal{H}_{J-1}$–null sets.

Each stratum $\partial\mathcal{R}_{\text{LSW}}(S)$ is a smooth $(|S|-1)$–dimensional ellipsoidal surface embedded in $\mathbb{R}^J$. On $\partial\mathcal{R}_{\text{LSW}}(S)$ the gradient of the defining function $F(w) := \sum_{j \in S} a_j w_j^2$ is $\nabla F(w) = (2a_1 w_1 \mathbf{1}\{1 \in S\}, \ldots, 2a_J w_J \mathbf{1}\{J \in S\})^\top$. Hence the outward unit normal vector is

$$n(w) = -\frac{(a_j w_j \mathbf{1}\{j \in S\})_{j=1}^J}{\sqrt{\sum_{j \in S} a_j^2 w_j^2}}, \qquad w \in \partial\mathcal{R}_{\text{LSW}}(S). \tag{21}$$

First derivative of local power. Using the boundary representation in Lemma 1.1, the first derivative of local power decomposes as

$$\pi'_{\text{LSW}}(0; h) = -\sum_{\emptyset \neq S \subset \{1,\ldots,J\}} \int_{\partial\mathcal{R}_{\text{LSW}}(S)} (\mu_h^\top n(w)) \, \varphi_\Sigma(w) \, d\mathcal{H}_{J-1}(w). \tag{22}$$

Only strata S that intersect the support of the negative drift $\{j : \mu_{h,j} < 0\}$ contribute nontrivially. Because $\mu_{h,j} \leq 0$ for all j, the integrand is positive precisely where the Gaussian mass concentrates on boundary points whose outward normal aligns with the negative drift direction. In contrast to LMW, the contribution is distributed "continuously" along the boundary rather than concentrated on coordinate-wise faces.

Second derivative of local power. Similarly, the second derivative admits the decomposition

$$\pi''_{\mathrm{LSW}}(0;h) = -\sum_{\emptyset \neq S \subset \{1,\dots,J\}} \int_{\partial \mathcal{R}_{\mathrm{LSW}}(S)} (\mu_h^\top n(w))(\mu_h^\top \Sigma^{-1} w)\, \varphi_\Sigma(w)\, d\mathcal{H}_{J-1}(w). \tag{23}$$

Relative to LMW, the curvature term now depends on the full geometry of the level set $\partial \mathcal{R}_{\mathrm{LSW}}$, reflecting the fact that LSW aggregates information across contacts instead of reacting to a single extremal direction.

The active–set decomposition shows that LSW aggregates local power contributions across all combinations of simultaneously binding contacts. Each stratum corresponds to a different pattern of joint violations, and the total local power is obtained by integrating Gaussian surface mass over all such strata. This contrasts with LMW, where only one–dimensional faces (single active constraints) appear, and anticipates the ELR case, where the active sets are determined endogenously by cone projection.

1.3.7 Application to ELR

We now apply the generalized Stein boundary representations to the ELR limiting experiment. In contrast to the LMW and LSW statistics, the ELR limit is naturally expressed as a quadratic distance to a convex cone under the Mahalanobis geometry induced by the long–run covariance matrix. This makes it convenient to work in whitened coordinates, where the Gaussian measure becomes spherical while the inequality cone becomes oblique.

Whitening. Let $W \sim N(0, \Sigma)$ with Σ positive definite and define

$$Q_\Sigma(W) := \inf_{\eta \in \mathbb{R}^J_+} (W - \eta)^\top \Sigma^{-1} (W - \eta).$$

This is the squared Mahalanobis-type distance from W to the nonnegative orthant. Introduce the whitened variable $V := \Sigma^{-1/2} W \sim N(0, I_J)$, $\tilde{\mu}_h := \Sigma^{-1/2}\mu_h$. For $\eta \geq 0$ set $\xi := \Sigma^{-1/2}\eta$. Then

$$Q_\Sigma(W) = \inf_{\xi \in K_\Sigma} \|V - \xi\|^2, \qquad K_\Sigma := \Sigma^{-1/2}\mathbb{R}^J_+.$$

Thus ELR is the squared Euclidean distance from V to the oblique cone K_Σ.

Boundary, active sets decomposition, and outward normal. Let c_{ELR} denote the $(1-\alpha)$ quantile of this null distribution. The rejection region in whitened coordinates is

$$\mathcal{R}_{\mathrm{ELR}} = \{v \in \mathbb{R}^J : \mathrm{dist}(v, K_\Sigma)^2 > c_{\mathrm{ELR}}\}.$$

Let the projection $\Pi_{K_\Sigma}(v) := \arg\min_{x \in K_\Sigma} \|v - \xi\|^2$, $r(v) := v - \Pi_{K_\Sigma}(v)$, then $\Psi_{\mathrm{ELR}}(v) = \|r(v)\|^2$. Since K_Σ is a closed convex polyhedral cone, the projection $\Pi_{K_\Sigma}(v)$ is uniquely defined and piecewise linear in v.

Write $G := \Sigma^{-1/2}$ and let g_j denote the jth column of G. Then $K_\Sigma = \mathrm{cone}\{g_1, \ldots, g_J\}$. For any subset $S \subset \{1, \ldots, J\}$ define the face $F_S := \mathrm{cone}\{g_j : j \in S\}$. For $\mathcal{H}_{J-1}$–almost every boundary point the projection $\Pi_{K_\Sigma}(v)$ lies in the relative interior of a unique face F_S. Define the corresponding boundary stratum $\partial\mathcal{R}_{\mathrm{ELR}}(S) := \left\{v : \Pi_{K_\Sigma}(v) \in \mathrm{ri}(F_S),\ \|r(v)\|^2 = c_{\mathrm{ELR}}\right\}$. Up to a Hausdorff measure null set, $\partial\mathcal{R}_{\mathrm{ELR}} = \bigcup_{S \subseteq \{1,\ldots,J\}} \partial\mathcal{R}_{\mathrm{ELR}}(S)$.

On each smooth stratum the gradient of the defining function $\Psi_{\mathrm{ELR}}(v) = \|r(v)\|^2$ is $\nabla\Psi_{\mathrm{ELR}}(v) = 2r(v)$, due to symmetry and idempotence of the linear operator $I_J - \Pi_{K_\Sigma}$. Hence the outward unit normal vector is

$$n(v) = -\frac{r(v)}{\sqrt{c_{\mathrm{ELR}}}} = \frac{\Pi_{K_\Sigma}(v) - v}{\sqrt{c_{\mathrm{ELR}}}}. \tag{24}$$

First derivative of local power. Applying the Gaussian boundary formula in whitened coordinates yields

$$\pi'_{\mathrm{ELR}}(0; h) = \frac{1}{\sqrt{c_{\mathrm{ELR}}}} \sum_{S \subseteq \{1,\ldots,J\}} \int_{\partial\mathcal{R}_{\mathrm{ELR}}(S)} \tilde{\mu}_h^\top r(v) \varphi_{I_J}(v)\, d\mathcal{H}_{J-1}(v), \tag{25}$$

where φ_{I_J} is the standard Gaussian density.

Second derivative of local power. Similarly,

$$\pi''_{\mathrm{ELR}}(0; h) = \frac{1}{\sqrt{c_{\mathrm{ELR}}}} \sum_{S \subseteq \{1,\ldots,J\}} \int_{\partial\mathcal{R}_{\mathrm{ELR}}(S)} (\tilde{\mu}_h^\top r(v))(\tilde{\mu}_h^\top v) \varphi_{I_J}(v)\, d\mathcal{H}_{J-1}(v). \tag{26}$$

The ELR rejection boundary consists of points at a fixed Euclidean distance from the oblique cone K_Σ. At each boundary point, the residual vector $r(v) := v - \Pi_{K_\Sigma}(v)$ points away from the cone along the shortest path and is orthogonal to the active face onto which v projects. The outward unit normal to the rejection boundary is the normalized vector $-r(v)/\sqrt{c_{\mathrm{ELR}}}$, while $r(v)$ itself points in the direction of increasing distance from the cone. Local power is therefore determined by the alignment between the whitened drift $\tilde{\mu}_h$ and the residual direction $r(v)$, weighted by the Gaussian surface density.

Notice, first, that the residual direction varies continuously along each smooth boundary stratum because it depends on the projection point $\Pi_{K_\Sigma}(v)$. This geometry allows ELR to combine information from several contact coordinates simultaneously through the active-face structure of the cone.

Second, the cone K_Σ encodes the covariance structure. After whitening, directions corresponding to highly variable linear combinations of the original moments are compressed, while directions with small variance are stretched. Consequently, the geometry of the cone and the associated Gaussian surface measure depend explicitly on Σ. Boundary regions corresponding to directions that are more informative relative to the covariance structure receive greater weight under the Mahalanobis geometry.

Consequently, ELR reallocates Gaussian surface mass toward directions where the drift is most informative relative to the covariance structure. This reweighting mechanism is expected to produce larger boundary integrals, and hence stronger local-power responses, for a substantial range of drift orientations.

1.3.8 Evaluation and comparison in the scalar binding case ($J = 1$)

This subsection evaluates the general Gaussian–shift derivatives derived above in the scalar case $J = 1$ and compares the three competing procedures. This clarifies that all differences between the limiting size adjusted LMW, LSW, and ELR are intrinsically multidimensional phenomena that only arise when $J > 1$.

First, and because $J = 1$, all three tests reduce to monotone functions of the same scalar quantity $-W$. Hence, for LMW, LSW, and ELR alike, the rejection region takes the form

$$\mathcal{R} = \{w \in \mathbb{R} : \; -w > c\} = (-\infty, -c), \qquad c > 0,$$

with c chosen to ensure size α. Thus, in the scalar case, all three tests share the same rejection set up to a relabeling of the critical value. The boundary is the singleton $\partial\mathcal{R} = \{-c\}$, $n(-c) = 1$, where $n(\cdot)$ denotes the outward unit normal. Using then the boundary Stein representation (15),

$$\pi'(0) = -\int_{\partial\mathcal{R}} (\mu_h n(w))\, \varphi_\sigma(w)\, d\mathcal{H}_0(w) = -\mu_h\, \varphi_\sigma(-c).$$

Also, from the boundary formula (16),

$$\pi''(0) = -(\mu_h n(-c))(\mu_h \sigma^{-2}(-c))\varphi_\sigma(-c) = \mu_h^2 \frac{c}{\sigma^2}\, \varphi_\sigma(-c) > 0.$$

Since, rejection regions and outward normals coincide, and the Gaussian surface density is identical across cases, the derivatives $\pi'(0)$ and $\pi''(0)$ are identical for LMW, LSW, and ELR up to test-specific rescalings of the critical value c that enforce size α. Consequently, under size correction,

$$\pi^{(k)}_{\mathrm{LMW}}(0;h) = \pi^{(k)}_{\mathrm{LSW}}(0;h) = \pi^{(k)}_{\mathrm{ELR}}(0;h), \qquad k = 1,2.$$

Thus $J = 1$, the three asymptotic procedures are locally equivalent: their rejection regions, boundary geometry, and Gaussian shift derivatives coincide. All distinctions between the size-corrected limiting LMW, LSW, and ELR therefore arise exclusively from multidimensional boundary geometry—namely, from how normals vary across active faces and how Gaussian mass is distributed along those faces when $J > 1$.

1.4 Gaussian Local Power under Structured Covariance

This section studies the local power properties of the LMW, LSW, and ELR tests under Gaussian limits with covariance structures that reflect the asymptotic behavior of stochastic dominance (SD) moment functions when $J > 1$.

Structured covariance. The covariance matrices arising in SSD applications typically exhibit pronounced heteroskedasticity together with strong positive dependence between neighboring moment functions, reflecting the fact that nearby inequalities are constructed from heavily overlapping integrals of the same empirical process. We write

$$\Sigma = D^{1/2} R D^{1/2},$$

where $D = \mathrm{diag}(\sigma_1^2, \ldots, \sigma_J^2)$ captures heteroskedasticity and R is a correlation matrix with large entries for nearby indices and weaker dependence for distant ones.

Oblique cone and generators. As above, passing to whitened coordinates, $V = \Sigma^{-1/2} W \sim N(0, I_J)$, the constraint set becomes the oblique cone $K_\Sigma = \Sigma^{-1/2}\mathbb{R}^J_+ = \mathrm{cone}(g_1, \ldots, g_J)$, $g_j := \Sigma^{-1/2} e_j$. Because $\Sigma^{-1/2}$ is invertible, the generators $\{g_j\}_{j=1}^J$ are linearly independent and K_Σ is a simplicial cone.

However, due to strong local dependence in Σ, neighboring generators g_j and g_{j+1} are typically close in direction. Thus, while the cone is globally full-dimensional, it is locally close to lower-dimensional along faces generated by neighboring contacts. This local near-collinearity is the key geometric feature induced by SD covariance structures.

Polar cone and ELR geometry. The dual geometry is described by the polar cone

$$K_\Sigma^\circ := \{y \in \mathbb{R}^J : y^\top x \le 0 \text{ for all } x \in K_\Sigma\}.$$

The polar cone collects outward normal directions to K_Σ. In particular, for almost every boundary point of the ELR rejection region, the projection residual $r(v) := v - \Pi_{K_\Sigma}(v)$ belongs to K_Σ° and determines the outward normal direction.

The ELR first-order local-power derivative can therefore be written as

$$\pi'_{\mathrm{ELR}}(0;\mu) = -\frac{1}{\sqrt{c_{\mathrm{ELR}}}} \int_{\partial\mathcal{R}_{\mathrm{ELR}}} d^\top r(v)\, \varphi(v)\, d\mathcal{H}_{J-1}(v),\ d := -\Sigma^{-1/2}\mu_h.$$

This representation shows that ELR power is governed by the alignment of the drift direction d with the polar cone K_Σ°.

Interior alignment and signal strength. A necessary and sufficient condition for strict interior alignment is $d \in \mathrm{int}(K_\Sigma)$, equivalently, $y^\top d < 0$ for all $y \in K_\Sigma^\circ \setminus \{0\}$.

Quantitatively, define the interiority margin $m(d; K_\Sigma^\circ) := \inf_{y \in K_\Sigma^\circ \cap S^{J-1}} (-y^\top d)$, where S^{J-1} denotes the unit sphere. Then $m(d; K_\Sigma^\circ) > 0$ if and only if $d \in \mathrm{int}(K_\Sigma)$. Moreover, since K_Σ is simplicial, every $d \in K_\Sigma$ admits a unique representation $d = \sum_{j=1}^J \lambda_j g_j,\ \lambda_j \ge 0$. Using the linearity of the boundary integral representation, $\pi'_{\mathrm{ELR}}(0;h) = \sum_{j=1}^J \lambda_j A(g_j)$, where $A(g_j) := -\frac{1}{\sqrt{c_{\mathrm{ELR}}}} \int_{\partial\mathcal{R}_{\mathrm{ELR}}} g_j^\top r(v)\, \varphi(v)\, d\mathcal{H}_{J-1}(v)$, with $r(v) = v - \Pi_{K_\Sigma}(v)$. Since $r(v) \in K_\Sigma^\circ$, $g_j \in K_\Sigma$, we have $g_j^\top r(v) \le 0$, and therefore $A(g_j) \ge 0$. Thus the ELR signal is a conic combination of contributions associated with the generators of K_Σ.

This decomposition provides a precise interpretation of the notion of "signal strength exploitable by ELR": generators g_j for which $A(g_j)$ is large correspond to directions along which the Gaussian surface measure concentrates and the ELR boundary is most sensitive.

Implications for drift directions. The ELR advantage arises whenever the reflected whitened drift d lies well inside the cone and places weight on generators with large boundary contributions $A(g_j)$.

Parallel drift $\mu = a\mathbf{1}$ is a canonical example: in that case $d = -\Sigma^{-1/2}\mu_h = |a| \sum_{j=1}^J g_j$, which lies in the relative interior of K_Σ and distributes weight across all generators. This produces strong alignment with the polar cone and a large ELR surface integral.

More generally, drifts that spread across several neighboring contacts remain well aligned with the cone geometry and generate strong ELR signal, especially when those contacts correspond to generators with similar direction due to local dependence.

By contrast, drifts concentrated on a small subset of contacts correspond to directions d that lie close to low-dimensional faces of K_Σ. In this case, d becomes nearly orthogonal to a nontrivial subset of polar directions, so that $-d^\top r(v)$ is small on boundary regions carrying substantial Gaussian mass. This weakens the ELR local-power derivative.

Comparison with LMW and LSW. This geometric mechanism explains the relative performance of the competing tests. The LMW statistic reacts to coordinatewise extrema and therefore does not exploit the dependence structure encoded in Σ. The LSW statistic aggregates components using fixed Euclidean weights, but does not adapt to the oblique geometry induced by $\Sigma^{-1/2}$.

In contrast, ELR fully internalizes the Mahalanobis geometry: its rejection region and boundary normals are defined through projection onto K_Σ, and its local power is driven by alignment with the polar cone. As a result, ELR is particularly effective when violations are distributed across directions that correspond to high-signal regions of the boundary under the Gaussian measure.

2 Additional empirical tests and details

2.1 Condor strategy details

Case	J	Condor	$K_{j,1}$	$K_{j,2}$	$K_{j,3}$	$K_{j,4}$
Slack ($T = 300$)	1	1	0.9811	0.9900	1.0100	1.0189
Slack ($T = 1000$)	1	1	0.9807	0.9900	1.0100	1.0193
Slack ($T = 3000$)	1	1	0.9805	0.9900	1.0100	1.0195
Binding	1	1	0.9802	0.9900	1.0100	1.0198
Binding	2	1	0.9731	0.9900	1.0100	1.0269
		2	1.0372	1.0500	1.0700	1.0828
Binding	3	1	0.9138	0.9300	0.9500	0.9662
		2	0.9740	0.9900	1.0100	1.0260
		3	1.0318	1.0500	1.0700	1.0882
Violated ($T = 300$)	3	1	0.9124	0.9300	0.9500	0.9676
		2	0.9743	0.9900	1.0100	1.0257
		3	1.0317	1.0500	1.0700	1.0883
Violated ($T = 1000$)	3	1	0.9130	0.9300	0.9500	0.9670
		2	0.9742	0.9900	1.0100	1.0258
		3	1.0318	1.0500	1.0700	1.0882
Violated ($T = 3000$)	3	1	0.9133	0.9300	0.9500	0.9667
		2	0.9741	0.9900	1.0100	1.0259
		3	1.0318	1.0500	1.0700	1.0882

Table 1: Condor strike prices for the Slack, Binding, and Violated dominance cases. Each row reports one condor spread, so cases with J condors occupy J rows. The Slack case is based on a single condor spread ($J = 1$) with maximum slack size $\Delta_0(T) = \frac{1}{2}\hat{\sigma}(x - y)T^{-1/2}$ for $T = 300, 1000$, and 3000, which drifts toward zero from above at rate $\sqrt{T}$. The Binding case is based on $J = 1, 2$, and 3 condor spreads with no slack ($\Delta_0(T) = 0$) and is therefore invariant to the sample size T. The Violated case is based on three condor spreads ($J = 3$) with a maximum violation of $\Delta_0(T) = -\frac{1}{2}\hat{\sigma}(x - y)T^{-1/2}$ for $T = 300, 1000$, and 3000, which drifts toward zero from below at rate $\sqrt{T}$. The strikes are constructed by sequentially increasing the outer strike range $K_{j,4} - K_{j,1}$ symmetrically around the inner strike range $K_{j,3} - K_{j,2}$ until the jth contact point is reached.

2.2 Sensitivity to test parameters.

SD Inequalities	Test	Param.	$T = 300$	$T = 1000$	$T = 3000$
Binding (3)	LMW	$b_0 = 0.6$	8.0	6.9	5.4
	LMW	$b_0 = 0.7$	8.8	7.3	5.9
	LMW	$b_0 = 0.8$	11.1	9.1	7.8
	LSW	$c_0 = 2^{-8}$	4.6	4.1	3.4
	LSW	$c_0 = 2^{-9}$	16.8	14.0	9.6
	LSW	$c_0 = 2^{-10}$	34.1	30.9	28.9
	ELR	$d_0 = 1$	9.9	10.0	9.9
	ELR	$d_0 = 2$	9.7	9.9	9.9
	ELR	$d_0 = 3$	9.7	9.9	9.9
Violated (3)	LMW	$b_0 = 0.6$	22.7	20.1	19.1
	LMW	$b_0 = 0.7$	25.0	21.3	20.3
	LMW	$b_0 = 0.8$	30.2	25.9	23.8
	LSW	$c_0 = 2^{-8}$	16.2	15.2	15.0
	LSW	$c_0 = 2^{-9}$	30.7	29.4	28.7
	LSW	$c_0 = 2^{-10}$	46.1	45.2	43.2
	ELR	$d_0 = 1$	35.4	38.2	38.8
	ELR	$d_0 = 2$	35.4	38.1	38.6
	ELR	$d_0 = 3$	35.4	38.1	38.6
Infeasible (3)	LMW	$b_0 = 0.6$	30.0	27.9	28.8
	LMW	$b_0 = 0.7$	30.0	27.9	28.8
	LMW	$b_0 = 0.8$	30.0	27.9	28.8
	LSW	$c_0 = 2^{-8}$	32.9	31.7	32.7
	LSW	$c_0 = 2^{-9}$	32.9	31.7	32.7
	LSW	$c_0 = 2^{-10}$	32.9	31.7	32.7
	ELR	$d_0 = 1$	35.1	37.3	38.9
	ELR	$d_0 = 2$	35.1	37.3	38.9
	ELR	$d_0 = 3$	35.1	37.3	38.9

Table 2: Sensitivity to test parameters. Entries are rejection rates in percent. The Binding (3) panel reports empirical size for the three-contact boundary null at the nominal 10% level, and the Violated (3) panel reports feasible power for the corresponding local three-contact violation. The table varies one tuning parameter at a time: the subsample exponent b_0 for LMW, the trimming constant c_0 for LSW, and the localization constant d_0 for ELR. The baseline values are $b_0 = 0.7$, $c_0 = 2^{-9}$, and $d_0 = 2$. All results use the equal drift vector $v = (1, 1, 1)'$ and grid size $m_T = \lfloor T^{0.6} \rfloor$. Results are based on 5000 Monte Carlo replications and 1000 resampling replications.

Table 2 studies sensitivity to the main test parameters while holding the grid fixed at $m_T = \lfloor T^{0.6} \rfloor$ and using the equal-drift specification. For LMW, we vary the subsample-length exponent b_0; for LSW, the trimming constant c_0; and for ELR, the localization constant d_0.

For LMW, increasing b_0 raises rejection rates under both Binding (3) and Violated (3). This partly mitigates the test's conservatism, but does not remove it. Even with the largest subsample exponent considered, LMW remains below or close to nominal size for the binding design, especially at larger sample sizes. The corresponding increase in power under Violated (3) is modest, and feasible power remains well below the size-adjusted oracle benchmark in Table 2. This is consistent with the baseline interpretation: LMW is affected by conservative critical-value estimation and by the volatility of the supremum statistic.

For LSW, the results reveal a more fundamental tuning problem. The rejection rates are highly sensitive to the trimming constant c_0, and no single value considered here delivers reliable size control across the relevant binding designs and sample sizes. The largest trimming constant, $c_0 = 2^{-8}$, is conservative under Binding (3), with rejection rates of 4.6, 4.1, and 3.4 percent, and also yields low power under Violated (3). The baseline value, $c_0 = 2^{-9}$, was chosen because it gives approximately correct size for Binding (3) at $T = 3000$, but it still overrejects under Binding (3) at smaller sample sizes and, as shown in Table 2, under Binding (2) as well. The smallest trimming constant, $c_0 = 2^{-10}$, produces much higher rejection rates under Violated (3), but this cannot be interpreted as a genuine power gain because it is accompanied by severe size distortions under Binding (3), with rejection rates of 34.1, 30.9, and 28.9 percent. Thus the feasible LSW procedure is not merely sensitive to a tuning parameter; the trimming value required for size control appears to depend on both the sample size and the number of binding contact points. This makes the feasible power of LSW difficult to interpret, because changes in rejection rates confound local power with failures of contact-set selection.

For ELR, rejection rates are essentially unchanged across $d_0 = 1, 2, 3$. Under Binding (3), all three localization constants deliver rejection rates very close to the nominal 10 percent level for all sample sizes. Under Violated (3), feasible power is also nearly identical across the three values of d_0. This robustness is important because the localization rule is intended to identify structurally relevant local minima rather than all nearly binding inequalities. The stability across d_0 suggests that the ELR implementation is not driven by delicate tuning of the localization threshold.

Overall, Table 2 shows that LMW is moderately sensitive to subsample length, LSW is highly sensitive to trimming, and ELR is robust to the localization constant. This supports the use of $d_0 = 2$ as the baseline ELR specification.

2.3 Sensitivity to grid size

SD Inequalities	Test	Param.	Grid	$T = 300$	$T = 1000$	$T = 3000$
Binding (3)	LMW	$b_0 = 0.7$	$\lfloor T^{0.5} \rfloor$	10.2	7.2	6.6
	LMW		$\lfloor T^{0.6} \rfloor$	8.8	7.3	5.9
	LMW		$\lfloor T^{0.7} \rfloor$	8.5	7.2	5.8
	LSW	$c_0 = 2^{-9}$	$\lfloor T^{0.5} \rfloor$	18.3	15.7	12.9
	LSW		$\lfloor T^{0.6} \rfloor$	16.8	14.0	9.6
	LSW		$\lfloor T^{0.7} \rfloor$	13.2	9.7	8.1
	ELR	$d_0 = 2$	$\lfloor T^{0.5} \rfloor$	8.7	8.9	10.0
	ELR		$\lfloor T^{0.6} \rfloor$	9.7	9.9	9.9
	ELR		$\lfloor T^{0.7} \rfloor$	9.8	10.1	9.9
Violated (3)	LMW	$b_0 = 0.7$	$\lfloor T^{0.5} \rfloor$	27.0	21.1	21.7
	LMW		$\lfloor T^{0.6} \rfloor$	25.0	21.3	20.3
	LMW		$\lfloor T^{0.7} \rfloor$	24.0	20.8	19.6
	LSW	$c_0 = 2^{-9}$	$\lfloor T^{0.5} \rfloor$	31.2	29.4	29.0
	LSW		$\lfloor T^{0.6} \rfloor$	30.7	29.4	28.7
	LSW		$\lfloor T^{0.7} \rfloor$	29.9	29.1	28.5
	ELR	$d_0 = 2$	$\lfloor T^{0.5} \rfloor$	32.6	34.6	38.8
	ELR		$\lfloor T^{0.6} \rfloor$	35.4	38.2	38.8
	ELR		$\lfloor T^{0.7} \rfloor$	36.4	38.2	38.9
Infeasible (3)	LMW	$b_0 = 0.7$	$\lfloor T^{0.5} \rfloor$	28.3	28.1	28.8
	LMW		$\lfloor T^{0.6} \rfloor$	30.0	27.9	28.8
	LMW		$\lfloor T^{0.7} \rfloor$	28.9	27.8	28.8
	LSW	$c_0 = 2^{-9}$	$\lfloor T^{0.5} \rfloor$	32.6	31.9	32.6
	LSW		$\lfloor T^{0.6} \rfloor$	32.9	31.7	32.7
	LSW		$\lfloor T^{0.7} \rfloor$	32.9	31.7	32.7
	ELR	$d_0 = 2$	$\lfloor T^{0.5} \rfloor$	34.2	36.9	39.1
	ELR		$\lfloor T^{0.6} \rfloor$	35.1	37.3	38.9
	ELR		$\lfloor T^{0.7} \rfloor$	35.9	37.0	39.2

Table 3: Sensitivity to grid size. Entries are rejection rates in percent. The Binding (3) panel reports empirical size for the three-contact boundary null at the nominal 10% level, and the Violated (3) panel reports feasible power for the corresponding local three-contact violation. The table varies the grid size $m_T = \lfloor T^{m_0} \rfloor$ over $m_0 \in \{0.5, 0.6, 0.7\}$, with $m_0 = 0.6$ as the baseline. The test parameters are fixed at their baseline values: $b_0 = 0.7$ for LMW, $c_0 = 2^{-9}$ for LSW, and $d_0 = 2$ for ELR. All results use the equal drift vector $v = (1, 1, 1)'$. Results are based on 5000 Monte Carlo replications and 1000 resampling replications.

Table 3 examines sensitivity to the granularity of the constraint grid, using $m_T = \lfloor T^{m_0} \rfloor$ with $m_0 \in \{0.5, 0.6, 0.7\}$. The baseline specification uses $m_0 = 0.6$. The comparison keeps the main test parameters fixed at $b_0 = 0.7$ for LMW, $c_0 = 2^{-9}$ for LSW, and $d_0 = 2$ for ELR.

For LMW, changing the grid size has only a modest effect. The test remains conservative under Binding (3) for all grid choices and sample sizes. Feasible power under Violated (3) is also relatively insensitive to the grid, and remains below the corresponding size-adjusted oracle benchmark. This is consistent with the fact that LMW is driven by the most adverse empirical coordinate; once the grid is sufficiently fine to capture the relevant neighborhood of the contact points, further grid refinement has limited impact on the supremum statistic.

For LSW, grid size interacts strongly with trimming-based contact selection. Under Binding (3), rejection rates decline as the grid becomes finer, especially for larger sample sizes. This confirms that LSW size control depends not only on the trimming constant c_0, but also on how the grid affects the set of inequalities classified as nearly binding. Although power under Violated (3) is relatively stable across grid choices, the size variation under Binding (3) means that feasible LSW rejection rates cannot be interpreted independently of the particular trimming and grid combination used.

For ELR, size control is stable across grid choices. Under Binding (3), rejection rates remain close to the nominal 10 percent level for all values of m_0. Under Violated (3), ELR power is somewhat lower for the coarsest grid when $T = 300$ and $T = 1000$, but the difference largely disappears for larger samples and for the two finer grids. This pattern is consistent with the localization strategy: the grid must be fine enough to place candidate points near the local minima of the gap function, but once this is achieved, further refinement has little effect because the selected nearby minima are highly collinear and span essentially the same local constraint space.

Overall, Table 3 shows that the main conclusions are not driven by a particular grid choice. LMW remains conservative, LSW remains more sensitive to the interaction between grid granularity and contact selection, and ELR maintains accurate size control and high feasible power across the grid specifications considered.

2.4 Localization accuracy

		Binding (3)			Violated (3)		
d_0	# locals	$T = 300$	$T = 1000$	$T = 3000$	$T = 300$	$T = 1000$	$T = 3000$
1	0	5.1	5.2	4.8	0.5	0.6	0.4
	1	9.1	8.7	8.9	2.7	2.3	2.0
	2	16.1	15.3	14.9	6.1	5.4	5.6
	3	69.8	70.7	71.4	90.7	91.7	91.9
	≥ 4	0.0	0.0	0.0	0.0	0.0	0.0
2	0	0.4	0.4	0.3	0.0	0.0	0.0
	1	1.2	1.2	1.2	0.1	0.2	0.1
	2	4.2	3.8	3.9	0.6	0.6	0.5
	3	94.2	94.6	94.6	99.3	99.2	99.3
	≥ 4	0.0	0.0	0.0	0.0	0.0	0.0
3	0	0.0	0.0	0.0	0.0	0.0	0.0
	1	0.0	0.1	0.1	0.0	0.0	0.0
	2	0.3	0.4	0.4	0.0	0.1	0.0
	3	99.6	99.5	99.6	100.0	100.0	100.0
	≥ 4	0.0	0.0	0.0	0.0	0.0	0.0

Table 4: Localization frequency for the ELR test. Entries are percentages across 5000 Monte Carlo replications. The table reports the simulated distribution of the number of candidate local minima selected by the ELR localization rule. The Binding (3) design has three true null contact points, where $\Delta(z) = 0$. The Violated (3) design has three target local minima at which the dominance inequalities are violated, where $\Delta(z) < 0$. Thus, in the Binding (3) case the selected minima correspond to candidate binding constraints, whereas in the Violated (3) case they correspond to candidate violation points. The table reports localization constants $d_0 = 1, 2, 3$. The grid size is $m_T = \lfloor T^{0.6} \rfloor$.

Table 4 reports the simulated distribution of the number of candidate local minima selected by the ELR localization rule for the Binding (3) and Violated (3) designs. In the Binding (3) design, the three target points are true contact points of the null, with $\Delta(z) = 0$. In the Violated (3) design, the three target points are instead local minima at which the dominance inequalities are violated, with $\Delta(z) < 0$. Thus, the table assesses whether the localization rule selects the relevant local minima of the gap function, both when they correspond to binding null constraints and when they correspond to local violations under the alternative.

For the baseline localization constant $d_0 = 2$, the procedure selects all three target minima with high frequency in both designs. Under Binding (3), the probability of selecting exactly three candidate minima is 94.2, 94.6, and 94.6 percent for $T = 300, 1000, 3000$, respectively. Under Violated (3), the corresponding frequencies are 99.3, 99.2, and 99.3 percent. Increasing the localization constant to $d_0 = 3$ essentially eliminates under-selection in these designs, while reducing it to $d_0 = 1$ leads to more frequent under-selection. Importantly, the procedure does not produce over-selection in these simulations: the number of selected minima never exceeds three. These results support the use of the baseline localization rule and explain the stability of the ELR size and power results with respect to d_0.

The distribution of localized constraints is slightly negatively skewed: underselection occurs more often than overselection. This is natural because the gap function $\Delta(z)$ is continuous and locally highly correlated, so the empirical curve tends to shift or bend rather than oscillate rapidly. Spurious local minima are therefore rare. By contrast, a true local minimum can disappear if two minima merge, if the curve locally flattens, or if an upward sampling shift moves it above the localization cutoff. This explains why almost all localization errors in Table 4 involve selecting fewer than three contacts rather than selecting too many.

This diagnostic helps explain the stability of the ELR rejection rates. Because the procedure localizes strict empirical minima rather than all near-binding inequalities, it avoids the instability that can arise in trimming-based procedures. Overselection is asymptotically less harmful because nearby selected minima are highly collinear and span essentially the same local constraint space. Underselection is more consequential because it can understate critical values, which is why using a moderately large localization constant is advisable. Overall, Table 4 supports the finite-sample reliability of the ELR critical-value procedure and explains why the rejection rates are largely insensitive to the localization constant in Table 2.

References

Arvanitis, S., Post, T., Potì, V., Karabati, S., 2021. Nonparametric tests for optimal predictive ability. International Journal of Forecasting 37, 881–898.

Doukhan, P., Massart, P., Rio, E., 1995. Invariance principles for absolutely regular empirical processes, in: Annales de l'IHP Probabilités et statistiques, pp. 393–427.

Fang, Z., Santos, A., 2019. Inference on directionally differentiable functions. The Review of Economic Studies 86, 377–412.

Linton, O., Song, K., Whang, Y.J., 2010. An improved bootstrap test of stochastic dominance. Journal of Econometrics 154, 186–202.

Peligrad, M., 1998. On the blockwise bootstrap for empirical processes for stationary sequences. The Annals of Probability 26, 877–901.

Rio, E., et al., 2017. Asymptotic theory of weakly dependent random processes. volume 80. Springer.

Appendix

This supplemental appendix contains the proofs of theoretical results along with auxiliary results regarding the asymptotics of the localization procedure and their proofs.

A Proofs

Proof of Theorem 1.1. The limit under $\mathbf{H}_0$ follows from the functional CLT for $\mathbb{G}_T$–see for example Th. 4 of Doukhan et al. (1995) along with Application 4 of Theorem 1 of the same paper, and the generalized (one-sided) delta method for the supremum functional over inequality constraints (see Fang and Santos (2019), together with the contact reduction: if $\Delta(z) > 0$ on a neighborhood, then $[-\Delta_T(z)]_+ = o_p(T^{-1/2})$ uniformly there. Under Pitman drifts, the limit is obtained by shifting the centering by h exploiting the applicability of a locally uniform (in the underlying measure) limit theorem. Under fixed alternatives, $\sup_z[-\Delta_T(z)]$ is bounded away from 0 w.p.a.1 and multiplied by $\sqrt{T}$ diverges. □

Proof of Theorem 1.2. Use the functional CLT for $\mathbb{G}_T$–see for example Th. 4 of Doukhan et al. (1995) along with Application 4 of Theorem 1 of the same paper, and the continuous mapping for the functional $f \mapsto \int [-f(z)]_+^2 \, \nu(dz)$ on $\ell^\infty(\mathcal{Z}_\infty)$, together with contact reduction as in Linton et al. (2010). Pitman drifts follow by shifting by h, again exploiting the applicability of a locally uniform (in the underlying measure) limit theory. Under fixed alternatives, the integral of squared violations is bounded away from 0 w.p.a.1 and scaling by T diverges again as in Linton et al. (2010). □

Proof of Theorem 1.3. The argument follows the proof strategy of Theorem 1 in Arvanitis et al. (2021), with the only additional ingredient being the stochastic, localized index set $\widehat{C}_T$.
Step 1 (PK-consistency of localization and reduction to contact coordinates). Under $\mathbf{H}_0$, Theorem B.1 in Appendix B. yields $\widehat{C}_T \xrightarrow{p} C$ in the PK sense, while under fixed alternatives

the localization concentrates on the strict-local-minima set $\mathcal{C}_\ell$. In particular, under $\mathbf{H}_0$ the selected moment vector coincides asymptotically (with $o_p(T^{-1/2})$ perturbations) with the vector of binding moments indexed by C, so that the asymptotic behavior of $\sqrt{T}\,\bar{\mathbf{g}}_{\widehat{C}_T,T}$ is governed by the same J-dimensional Gaussian limit as the corresponding contact vector $\sqrt{T}\,\bar{\mathbf{g}}_{C,T}$. Remarks B.1 and B.2 handle the limiting behavior of localization under fixed alternatives and Pitman drifts.

Step 2 (continuity/semicontinuity of the cone constraint under set convergence). The ELR statistic can be expressed in the standard self-normalized quadratic form after dualization and second-order expansion around $\lambda = 0$:

$$\mathrm{ELR}_T = \inf_{\eta\in\mathbb{R}^J_+} \big(\sqrt{T}\,\bar{\mathbf{g}}_{\widehat{C}_T,T} - \eta\big)^\top \widehat{\Sigma}_T^{-1} \big(\sqrt{T}\,\bar{\mathbf{g}}_{\widehat{C}_T,T} - \eta\big) + o_p(1),$$

where $\widehat{\Sigma}_T$ is the long-run covariance estimator on the selected coordinates. Because the feasible set $\mathbb{R}^J_+$ is a closed convex cone, the convex indicator functional is lower semicontinuous, and the corresponding projection map is nonexpansive; combined with PK convergence of $\widehat{C}_T$ and consistency of $\widehat{\Sigma}_T$, this yields stability of the constrained quadratic program under the random localization (i.e., replacing $\widehat{C}_T$ by C changes the objective by $o_p(1)$).

Step 3 (null and Pitman limits). Under $\mathbf{H}_0$, $\sqrt{T}\,\bar{\mathbf{g}}_{C,T} \rightsquigarrow W \sim N(0,\Sigma)$ by the β-mixing FCLT–see for example Th. 8.3 of Rio et al. (2017), hence the continuous mapping theorem applied to the cone-projection functional yields (7). Under Pitman drifts, the same argument applies with the Gaussian shift $W \mapsto W + \mu_h$, yielding (8). The local-uniformity assumption on Assumptions 1.1–1.2 ensures that the remainder terms in the quadratic expansion and the stochastic equicontinuity bounds can be controlled uniformly over the drifting sequence of measures, exactly as in Arvanitis et al. (2021).

Step 4 (fixed alternatives and $J = 0$). If $\Delta(z_0) < 0$ for some $z_0 \in \mathcal{Z}_\infty$, then at least one selected coordinate exhibits a fixed negative mean (either directly or via localization on strict minima), which forces the dual optimizer away from zero and implies $\mathrm{ELR}_T \to \infty$ by the standard EL divergence argument. If $J = 0$, then all inequalities are locally slack under $\mathbf{H}_0$, so the constrained and unconstrained optima coincide asymptotically and $\mathrm{ELR}_T \rightsquigarrow 0$. □

Proof of Proposition 1.1. (i) Subsampling consistency for functionals of weakly dependent empirical processes follows from standard subsampling theory under absolute regularity; the LMW functional is measurable and continuous at the limit process with probability one under the stated contact conditions. (ii) Divergence under fixed alternatives implies consistency; Pitman power follows by continuous mapping applied to the shifted process. □

Proof of Proposition 1.2. Let C denote the population contact set and let J_C be the corresponding grid index set. Since $c_T \to 0$ and $\sqrt{T}c_T \to \infty$, binding constraints satisfy $|\Delta_T(z)| = O_p(T^{-1/2}) = o_p(c_T)$, whereas strictly slack constraints have population gaps bounded away from zero and are excluded with probability tending to one. Hence, by the assumed separation of the contact set and the grid approximation condition, $\mathbb{P}\{J_T = J_C\} \to 1$.

On this event, the bootstrap statistic can be written as

$$\mathrm{LSW}_T^* = T \sum_{j \in J_C} w_{T,j}[-\{\Delta_T^*(z_{T,j}) - \Delta_T(z_{T,j})\}]_+^2 + o_p^*(1).$$

The ordinary bootstrap under independence, and the block bootstrap under dependence with $b_T \to \infty$, $b_T/T \to 0$, consistently estimate the centered empirical process on the finite contact set:

$$\sqrt{T}\{\Delta_T^*(z) - \Delta_T(z)\}_{z \in C} \rightsquigarrow_p \{\mathbb{G}(z)\}_{z \in C}.$$

Since $x \mapsto [-x]_+^2$ is continuous and the contact set is finite, the continuous mapping theorem yields

$$\mathrm{LSW}_T^* \rightsquigarrow_p \int_C [-\mathbb{G}(z)]_+^2 \, \nu(dz).$$

The convergence of the conditional quantile follows at continuity points of the limiting distribution, in particular at the relevant critical value under the usual no-atom condition.

The same weak limit holds for the full-sample statistic under the null, so if $J \geq 1$ the rejection probability converges to α. If $J = 0$, all dominance inequalities are strictly slack; hence the positive-part statistic converges to zero and the rejection probability vanishes.

Under a fixed alternative, there exists z_0 such that $\Delta(z_0) < 0$. By grid approximation, with probability tending to one there is a grid point near z_0, and the corresponding empirical gap remains negative and bounded away from zero. Therefore

$$\mathrm{LSW}_T = T \sum_j w_{T,j}[-\Delta_T(z_{T,j})]_+^2 \to \infty$$

in probability, provided the limiting measure assigns positive mass to the violating region. By contrast, the recentered bootstrap statistic is centered around Δ_T and remains governed by the centered empirical-process limit, so its critical values are $O_p(1)$. Consistency follows. □

Proof of Proposition 1.3. We give the proof for the nondegenerate null case $J \geq 1$. The degenerate and fixed-alternative cases follow at the end. Let $C = \{c_1, \dots, c_J\}$ denote the population contact set and write

$$Z_t := g_C(X_t, Y_t) \in \mathbb{R}^J, \qquad \bar{Z}_T := T^{-1} \sum_{t=1}^T Z_t.$$

By the consistency of the localization rule,

$$\widehat{C}_T \xrightarrow{p} C$$

in the Painlevé–Kuratowski topology. Hence, with probability tending to one, the localized EL problem is asymptotically equivalent to the same EL problem formed on C. It therefore suffices to prove the result for the fixed J-dimensional vector Z_t.

Let Z_t^* denote the block-bootstrap pseudo-series and define the recentered bootstrap mean

$$\bar{Z}_T^* := T^{-1} \sum_{t=1}^{T} Z_t^*, \qquad G_T^* := \sqrt{T}(\bar{Z}_T^* - \bar{Z}_T).$$

Under the stated mixing, moment and block-bootstrap conditions, the conditional bootstrap central limit theorem–see for example Peligrad (1998), gives

$$G_T^* \rightsquigarrow_p W, \qquad W \sim N(0, \Sigma),$$

Now form the overlapping bootstrap EL block averages

$$\bar{Z}_{s,\ell}^* := \ell_T^{-1} \sum_{t=s}^{s+\ell_T-1} Z_t^*, \qquad s = 1, \ldots, T_\ell,$$

and recenter them as

$$U_{s,\ell}^* := \bar{Z}_{s,\ell}^* - \bar{Z}_T.$$

The average of the block moments satisfies

$$\bar{U}_\ell^* := T_\ell^{-1} \sum_{s=1}^{T_\ell} U_{s,\ell}^* = \bar{Z}_T^* - \bar{Z}_T + o_p^*(T^{-1/2}),$$

the error being due only to endpoint effects and therefore negligible since $\ell_T/T \to 0$.

The relevant covariance estimator for the blockwise EL expansion is

$$S_{\ell,T}^* := \frac{\ell_T}{T_\ell} \sum_{s=1}^{T_\ell} \big(U_{s,\ell}^* - \bar{U}_\ell^*\big)\big(U_{s,\ell}^* - \bar{U}_\ell^*\big)^\top.$$

The moving-block bootstrap consistently reproduces the long-run covariance of the original process, and the additional compatibility condition $\ell_T/b_T \to 0$ ensures that the fraction of EL blocks crossing bootstrap resampling boundaries is asymptotically negligible. Indeed, each bootstrap boundary affects at most $O(\ell_T)$ overlapping EL blocks, while the number of bootstrap boundaries is $O_p(T/b_T)$. Hence the affected proportion is

$$O_p\left(\frac{(T/b_T)\ell_T}{T}\right) = O_p(\ell_T/b_T) = o_p(1).$$

Consequently,

$$S^*_{\ell,T} \xrightarrow{p^*} \Sigma$$

in probability. It remains to expand the bootstrap EL criterion. Let $\lambda^*_T \leq 0$ be the dual multiplier of the bootstrap EL problem on the localized contact set. The dual criterion is

$$\mathrm{ELR}^*_T = 2\sum_{s=1}^{T_\ell} \log\{1 + \lambda^{*\top}_T U^*_{s,\ell}\}.$$

The first-order condition implies

$$\lambda^*_T = -\frac{\ell_T}{T}\Sigma^{-1}\sqrt{T}(\bar{Z}^*_T - \bar{Z}_T) + o^*_p\left(\frac{\ell_T}{\sqrt{T}}\right),$$

uniformly on sets whose probability tends to one. Moreover,

$$\max_{1\leq s\leq T_\ell} \|U^*_{s,\ell}\| = O^*_p(T^{1/(2+\delta)}),$$

and therefore

$$\max_{1\leq s\leq T_\ell} |\lambda^{*\top}_T U^*_{s,\ell}| = O^*_p\big(\ell_T T^{1/(2+\delta)-1/2}\big) = o^*_p(1).$$

Thus the logarithm admits the uniform quadratic expansion

$$2\log(1+x) = 2x - x^2 + o(x^2),$$

applied with $x = \lambda^{*\top}_T U^*_{s,\ell}$. Hence

$$\mathrm{ELR}^*_T = T_\ell \bar{U}^{*\top}_\ell \left\{\frac{1}{T_\ell}\sum_{s=1}^{T_\ell} U^*_{s,\ell}U^{*\top}_{s,\ell}\right\}^{-1} \bar{U}^*_\ell + o^*_p\left(\frac{T_\ell \ell_T}{T}\right).$$

Multiplying by $a_T = T/(T_\ell \ell_T)$ gives

$$\mathrm{ELR}^*_T = \left\{\sqrt{T}(\bar{Z}^*_T - \bar{Z}_T)\right\}^\top \Sigma^{-1}\left\{\sqrt{T}(\bar{Z}^*_T - \bar{Z}_T)\right\} + o^*_p(1)$$

in the unrestricted equality case. For the inequality-constrained EL problem, the same quadratic expansion is taken over the tangent cone induced by the nonnegative moment restrictions. Equivalently, the unrestricted quadratic form is replaced by the squared Mahalanobis distance of the Gaussian mean perturbation from the nonnegative orthant:

$$\mathrm{ELR}_T^* = \inf_{\eta \in \mathbb{R}_+^J} \big(G_T^* - \eta\big)^\top \Sigma^{-1} \big(G_T^* - \eta\big) + o_p^*(1).$$

Since $G_T^* \rightsquigarrow_p W \sim N(0, \Sigma)$, and projection onto the closed convex cone $\mathbb{R}_+^J$ is continuous, the conditional continuous mapping theorem yields

$$\mathrm{ELR}_T^* \rightsquigarrow_p Q(\Sigma).$$

The convergence of conditional quantiles follows because the distribution function of $Q(\Sigma)$ is continuous at $c_\alpha(\Sigma)$, in particular for $\alpha < 1/2$. This proves part (i).

If $J = 0$, the population dominance gap is strictly slack. The localization rule selects no contact point with probability tending to one, so the localized ELR statistic is zero by convention. Hence

$$\mathrm{ELR}_T \rightsquigarrow 0$$

and the rejection probability tends to zero, proving part (ii).

Finally, suppose that

$$\inf_{z \in \mathcal{Z}_\infty} \Delta(z) < 0.$$

Then at least one finite localized minimum, or the mean point at infinity when included, has a strictly negative population gap. The empirical localized moment vector therefore has a component bounded away from zero in the violating direction with probability tending to one. The EL criterion consequently grows at order T, so that

$$\mathrm{ELR}_T \to \infty$$

in probability. By contrast, the recentered bootstrap statistic is computed after subtracting the full-sample localized moment vector and is therefore asymptotically boundary-centered. The preceding bootstrap argument then implies

$$\widetilde{c}^*_{\alpha,T} = O_p(1).$$

Thus the empirical statistic diverges while the bootstrap critical value remains bounded, and the test is consistent. This proves part (iii). □

Proof of Lemma 1.1. **Step 1: Differentiation under the integral (volume formulas).**

Since φ_Σ is C^∞ and μ is fixed, for each w the map $t \mapsto \varphi_\Sigma(w + t\mu)$ is C^∞ with

$$\frac{d}{dt}\varphi_\Sigma(w - t\mu_h) = -\mu_h^\top \nabla\varphi_\Sigma(w - t\mu_h), \qquad \frac{d^2}{dt^2}\varphi_\Sigma(w - t\mu_h) = \mu_h^\top \nabla^2\varphi_\Sigma(w - t\mu_h)\mu_h.$$

Under the stated integrability conditions, dominated convergence justifies differentiating under the integral sign at $t = 0$, giving

$$\pi'(0) = -\int_{\mathcal{R}} \mu_h^\top \nabla\varphi_\Sigma(w)\, dw, \qquad \pi''(0) = \int_{\mathcal{R}} \mu_h^\top \nabla^2\varphi_\Sigma(w)\mu_h\, dw.$$

Now use the standard Gaussian identities

$$\nabla\varphi_\Sigma(w) = -\varphi_\Sigma(w)\Sigma^{-1}w, \qquad \nabla^2\varphi_\Sigma(w) = \varphi_\Sigma(w)\big(\Sigma^{-1}ww^\top\Sigma^{-1} - \Sigma^{-1}\big),$$

to obtain (13) and (14) after rewriting the resulting integrals as expectations under $W \sim N(0, \Sigma)$.

Step 2: Divergence theorem for $\pi'(0)$ (boundary formula). Let $F_1(w) := -\mu_h\, \varphi_\Sigma(w)$. Then F_1 is continuously differentiable and

$$\nabla \cdot F_1(w) = -\sum_{j=1}^{J} \partial_j\big(\mu_{h,j}\varphi_\Sigma(w)\big) = -\mu_h^\top \nabla\varphi_\Sigma(w).$$

Since $\mathcal{R}$ has Lipschitz boundary and the relevant integrability holds, the divergence theorem applies:

$$\int_{\mathcal{R}} \mu_h^\top \nabla\varphi_\Sigma(w)\, dw = \int_{\mathcal{R}} \nabla \cdot F_1(w)\, dw = \int_{\partial\mathcal{R}} F_1(w) \cdot n(w)\, d\mathcal{H}_{J-1}(w).$$

Because $F_1(w) \cdot n(w) = -(\mu_h^\top n(w))\varphi_\Sigma(w)$, this yields (15).

Step 3: Divergence theorem for $\pi''(0)$ (boundary formula). Let $A := \mu_h\mu_h^\top$ and define $F_2(w) := A\,\nabla\varphi_\Sigma(w)$. Since A is constant and φ_Σ is C^∞,

$$\nabla \cdot F_2(w) = \sum_{i=1}^{J} \partial_i\Big(\sum_{j=1}^{J} A_{ij}\partial_j\varphi_\Sigma(w)\Big) = \sum_{i,j=1}^{J} A_{ij}\partial_{ij}\varphi_\Sigma(w) = \mu_h^\top \nabla^2\varphi_\Sigma(w)\mu_h.$$

Applying the divergence theorem again,

$$\int_{\mathcal{R}} \mu_h^\top \nabla^2\varphi_\Sigma(w)\mu_h\, dw = \int_{\mathcal{R}} \nabla \cdot F_2(w)\, dw = \int_{\partial\mathcal{R}} F_2(w) \cdot n(w)\, d\mathcal{H}_{J-1}(w).$$

Noting that $F_2(w) \cdot n(w) = n(w)^\top(\mu\mu_h^\top \nabla\varphi_\Sigma(w)) = (\mu_h^\top n(w))(\mu_h^\top \nabla\varphi_\Sigma(w))$ gives the first two equalities in (16). Substituting $\nabla\varphi_\Sigma(w) = -\varphi_\Sigma(w)\Sigma^{-1}w$ yields the last equality in (16).

Step 4: Taylor expansion of $\pi(t)$. A second-order Taylor expansion of $\varphi_\Sigma(w - t\mu_h)$ around $t = 0$ with remainder, combined with dominated convergence, yields

$$\pi(t) = \pi(0) + t\,\pi'(0) + \frac{t^2}{2}\pi''(0) + o(t^2),$$

completing the proof. $\square$

B Localization auxiliary results

Recall the finite-threshold localized estimator

$$\widehat{C}_{T,f} := \{z \in \mathcal{Z}_T :\; z \text{ is a discrete local minimum of } \Delta_T(\cdot) \text{ on } \mathcal{Z}_T,\; \Delta_T(z) \le d_T\}.$$

When the mean restriction is imposed, set $\widehat{C}_{T,\infty} := \{\infty\}$ if $\Delta_T(\infty) \le d_{T,\infty}$ and $\widehat{C}_{T,\infty} := \emptyset$ otherwise, where $d_{T,\infty} \downarrow 0$ and $\sqrt{T} d_{T,\infty} \to \infty$. If the mean restriction is not imposed, set $\widehat{C}_{T,\infty} := \emptyset$. The full localized set is

$$\widehat{C}_T := \widehat{C}_{T,f} \cup \widehat{C}_{T,\infty}.$$

Theorem B.1 (Localization of binding constraints)**.** *Suppose Assumptions 1.1–1.4 hold and $d_T \downarrow 0$ satisfies $\sqrt{T}\, d_T \to \infty$. Then, under $\mathbf{H}_0$:*

*(i) (*No spurious accumulation outside finite contacts.*) Writing $C_f = \{c_{f,1}, \dots, c_{f,J_f}\}$, for every $\varepsilon > 0$,*

$$\mathbb{P}\Big(\widehat{C}_{T,f} \subset C_f^{\varepsilon}\Big) \to 1, \qquad C_f^{\varepsilon} := \bigcup_{j=1}^{J_f} (c_{f,j} - \varepsilon, c_{f,j} + \varepsilon).$$

Equivalently, $\limsup_{T\to\infty} \widehat{C}_{T,f} \subseteq C_f$ in probability.

*(ii) (*No missed finite contacts.*) For each finite contact $c_{f,j} \in C_f$ and each sufficiently small $\varepsilon > 0$,*

$$\mathbb{P}\Big(\widehat{C}_{T,f} \cap (c_{f,j} - \varepsilon, c_{f,j} + \varepsilon) \neq \emptyset\Big) \to 1.$$

Equivalently, $C_f \subseteq \liminf_{T\to\infty} \widehat{C}_{T,f}$ in probability.

*(iii) (*PK convergence.*) For the finite component, $\widehat{C}_{T,f} \xrightarrow{p} C_f$ in the Painlevé–Kuratowski sense on $\mathcal{Z}$. For the infinity component, if the mean restriction is imposed and $\Delta(\infty) = 0$, then $\mathbb{P}(\widehat{C}_{T,\infty} = \{\infty\}) \to 1$; if the mean restriction is not imposed, or if it is imposed and $\Delta(\infty) > 0$, then $\mathbb{P}(\widehat{C}_{T,\infty} = \emptyset) \to 1$. Hence $\widehat{C}_T \xrightarrow{p} C$ in the corresponding augmented sense.*

Proof. We first prove the finite-threshold localization statements. Fix $\varepsilon > 0$ small enough that the neighborhoods of the finite contacts are contained in the corresponding neighborhoods from Assumption 1.3, and set

$$C_f^\varepsilon := \bigcup_{j=1}^{J_f} (c_{f,j} - \varepsilon, c_{f,j} + \varepsilon).$$

Choose $R > 0$ such that $C_f^\varepsilon \subset [-R, R]$.

Step 1 (separation away from C_f: using the level condition). Under $\mathbf{H}_0$, $\Delta(z) > 0$ on the compact set

$$K_\varepsilon := \mathcal{Z} \cap \big([-R, R] \setminus C_f^\varepsilon\big),$$

hence by continuity there exists

$$m_\varepsilon := \inf_{z \in K_\varepsilon} \Delta(z) \; > \; 0.$$

By stochastic equicontinuity / the uniform FCLT implied by Assumptions 1.1–1.2,

$$\sup_{z \in \mathcal{Z} \cap [-R,R]} \big|\Delta_T(z) - \Delta(z)\big| = O_p(T^{-1/2}),$$

so

$$\mathbb{P}\Big(\inf_{z \in K_\varepsilon} \Delta_T(z) \geq m_\varepsilon/2\Big) \to 1.$$

Because $d_T \downarrow 0$, for T large enough $d_T < m_\varepsilon/2$, hence on the above event no $z \in \mathcal{Z}_T \cap ([-R, R] \setminus C_f^\varepsilon)$ can satisfy $\Delta_T(z) \leq d_T$. Therefore, with probability $\to 1$,

$$\widehat{C}_{T,f} \cap [-R, R] \; \subseteq \; C_f^\varepsilon. \tag{27}$$

Assumption 1.4(i) ensures that eventually $[-R, R] \subset [-R_T, R_T]$ with probability $\to 1$, so (27) implies (i) for the finite component, since ε is arbitrary.

Step 2 (existence of a selected discrete local minimum near each finite contact). Fix a finite contact $c_{f,j} \in C_f$ and choose $\varepsilon > 0$ small enough that the interval

$$I_{j,\varepsilon} := (c_{f,j} - \varepsilon, c_{f,j} + \varepsilon)$$

is contained in the corresponding neighborhood from Assumption 1.3. By Assumption 1.4(ii), with probability $\to 1$ the grid $\mathcal{Z}_T$ contains at least one point in $I_{j,\varepsilon/2}$ and points on both sides of $c_{f,j}$ inside $I_{j,\varepsilon}$, so that interior grid points in $I_{j,\varepsilon/2}$ have well-defined left/right neighbors.

Let

$$A_T := \left\{ \sup_{z \in \mathcal{Z} \cap I_{j,\varepsilon}} |\Delta_T(z) - \Delta(z)| \leq \tfrac{1}{4}\kappa_j \varepsilon^2 \right\},$$

so $\mathbb{P}(A_T) \to 1$ by the same uniform approximation.

On A_T, for any $z \in \mathcal{Z} \cap I_{j,\varepsilon}$ we have

$$\Delta_T(z) \geq \Delta(z) - \tfrac{1}{4}\kappa_j \varepsilon^2 \geq \kappa_j (z - c_{f,j})^2 - \tfrac{1}{4}\kappa_j \varepsilon^2.$$

In particular, for any grid point $z \in \mathcal{Z}_T \cap I_{j,\varepsilon}$ with $|z - c_{f,j}| \geq \varepsilon/2$,

$$\Delta_T(z) \geq \kappa_j (\varepsilon/2)^2 - \tfrac{1}{4}\kappa_j \varepsilon^2 = \tfrac{1}{4}\kappa_j \varepsilon^2.$$

Whereas for any grid point $z^\star \in \mathcal{Z}_T \cap I_{j,\varepsilon/2}$,

$$\Delta_T(z^\star) \leq \Delta(z^\star) + \tfrac{1}{4}\kappa_j \varepsilon^2 \leq \kappa_j (\varepsilon/2)^2 + \tfrac{1}{4}\kappa_j \varepsilon^2 = \tfrac{1}{2}\kappa_j \varepsilon^2.$$

Thus, on A_T the *global* minimizer of Δ_T over the finite set $\mathcal{Z}_T \cap I_{j,\varepsilon}$ is attained at some $\tilde{z}_{T,j} \in \mathcal{Z}_T \cap I_{j,\varepsilon/2}$.

Now use *adjacency*: because $\tilde{z}_{T,j}$ minimizes Δ_T over $\mathcal{Z}_T \cap I_{j,\varepsilon}$, it is in particular no larger than its immediate neighbors in that set. If $\tilde{z}_{T,j}$ is an interior grid point within $I_{j,\varepsilon}$, then its adjacent neighbors $z_{T,i-1}, z_{T,i+1}$ satisfy

$$\Delta_T(\tilde{z}_{T,j}) \leq \Delta_T(z_{T,i-1}), \qquad \Delta_T(\tilde{z}_{T,j}) \leq \Delta_T(z_{T,i+1}),$$

so $\tilde{z}_{T,j}$ is a discrete local minimum in the sense of the definition. If the minimizer occurs at the first/last grid point inside $I_{j,\varepsilon}$, then the one-sided endpoint criterion applies by construction. Hence, with probability $\to 1$, $\tilde{z}_{T,j}$ is a discrete local minimum.

Finally, on A_T and since $\Delta(c_{f,j}) = 0$, we have $\Delta_T(\tilde{z}_{T,j}) = O_p(T^{-1/2})$; indeed, $\Delta_T(\tilde{z}_{T,j}) \leq \Delta_T(c^\dagger_{f,j})$ for any grid point $c^\dagger_{f,j} \to c_{f,j}$ and $\Delta_T(c^\dagger_{f,j}) = \Delta(c^\dagger_{f,j}) + O_p(T^{-1/2}) = O_p(T^{-1/2})$. Because $\sqrt{T}\, d_T \to \infty$, this implies

$$\mathbb{P}\big(\Delta_T(\tilde{z}_{T,j}) \leq d_T\big) \to 1,$$

hence $\tilde{z}_{T,j} \in \widehat{C}_{T,f}$ and $\tilde{z}_{T,j} \in I_{j,\varepsilon}$ with probability $\to 1$. This proves (ii) for the finite component.

Step 3 (finite PK convergence). Part (i) gives the outer PK condition and part (ii) gives the inner PK condition for the finite component, hence $\widehat{C}_{T,f} \xrightarrow{p} C_f$ in the Painlevé–Kuratowski sense on $\mathcal{Z}$.

Step 4 (infinity component). If the mean restriction is imposed and $\Delta(\infty) = 0$, then $\Delta_T(\infty) - \Delta(\infty) = O_p(T^{-1/2})$. Since $\sqrt{T} d_{T,\infty} \to \infty$, it follows that $\mathbb{P}(\Delta_T(\infty) \leq d_{T,\infty}) \to 1$, and hence $\mathbb{P}(\widehat{C}_{T,\infty} = \{\infty\}) \to 1$. If the mean restriction is imposed and $\Delta(\infty) > 0$, then $\Delta_T(\infty) \to_p \Delta(\infty) > 0$ while $d_{T,\infty} \downarrow 0$, so $\mathbb{P}(\Delta_T(\infty) \leq d_{T,\infty}) \to 0$, and therefore $\mathbb{P}(\widehat{C}_{T,\infty} = \emptyset) \to 1$. If the mean restriction is not imposed, $\widehat{C}_{T,\infty} = \emptyset$ by definition. Combining this scalar component with the finite PK convergence gives the stated convergence of the full localized set $\widehat{C}_T$ to $C = C_f \cup C_\infty$. □

Remark B.1 (PK behavior of the localization set under $\mathbf{H}_1$.). Theorem B.1 is stated under $\mathbf{H}_0$ with limit set $C = C_f \cup C_\infty$. Exactly the same finite-grid PK argument applies under a fixed alternative $\mathbf{H}_1$, with the finite limit set replaced by the finite set of strict local minima of the population gap function,

$$\mathcal{C}_\ell := \{c_1^\star, \dots, c_{J_\ell}^\star\},$$

as in Assumption 1.3. The possible violation of the mean restriction is handled separately through $\Delta(\infty)$. Indeed, fix $\varepsilon > 0$ and work on a compact $[-R, R]$ containing $\mathcal{C}_\ell^\varepsilon := \bigcup_{j=1}^{J_\ell}(c_j^\star - \varepsilon, c_j^\star + \varepsilon)$. Since Δ is continuous and $\mathcal{C}_\ell$ is finite, we have the separation bound

$$m_{\ell,\varepsilon} := \inf_{z \in \mathcal{Z} \cap ([-R,R] \setminus \mathcal{C}_\ell^\varepsilon)} \Delta(z) > 0.$$

Uniform approximation of Δ_T by Δ on $[-R, R]$ from Assumptions 1.1–1.2 then yields $\inf_{z \in [-R,R] \setminus \mathcal{C}_\ell^\varepsilon} \Delta_T(z) \geq m_{\ell,\varepsilon}/2$ w.p. $\to 1$, so the *level* condition $\Delta_T(z) \leq d_T$ rules out any selected finite grid point outside $\mathcal{C}_\ell^\varepsilon$ once $d_T < m_{\ell,\varepsilon}/2$, giving the outer PK condition. For the inner PK condition, the local quadratic growth (1) around each $c_j^\star$ implies that, on a high-probability uniform approximation event, the minimizer of Δ_T over the finite set $\mathcal{Z}_T \cap (c_j^\star - \varepsilon, c_j^\star + \varepsilon)$ lies in $(c_j^\star - \varepsilon/2, c_j^\star + \varepsilon/2)$. Since this point is a minimizer over the interval-restricted grid, it is in particular no larger than its adjacent grid neighbors there, hence it is a discrete local minimum in the sense used in the definition of $\widehat{C}_{T,f}$ with one-sided modifications at endpoints. Finally, the same argument as under $\mathbf{H}_0$ gives $\Delta_T(\tilde{z}_{T,j}) = O_p(T^{-1/2})$, so $\Delta_T(\tilde{z}_{T,j}) \leq d_T$ w.p. $\to 1$ because $\sqrt{T}\, d_T \to \infty$. Thus $\widehat{C}_{T,f} \xrightarrow{p} \mathcal{C}_\ell$ in the PK sense under $\mathbf{H}_1$. If the mean restriction is imposed and $\Delta(\infty) < 0$, then $\widehat{C}_{T,\infty} = \{\infty\}$ with probability tending to one.

Remark B.2 (Pitman drifts / local alternatives). Consider local alternatives of the form

$$\Delta_T^{(h,r_T)}(z) := \Delta(z) + T^{-1/2} h(z) + r_T(z), \qquad \sup_{z \in \mathcal{Z} \cap [-R,R]} |r_T(z)| = o(T^{-1/2})$$

on each compact $[-R, R]$, for some deterministic drift h that is continuous on $\mathcal{Z}$. Assume that the strict local minima of Δ are isolated and satisfy the quadratic growth condition (1), and that the drift does not destroy isolation, equivalently, the perturbed criterion $\Delta + T^{-1/2}h$ has the same number of local minima inside the neighborhoods N_j for all large T. Then the same separation/inner-minimizer argument yields that $\widehat{C}_{T,f}$ concentrates in vanishing neighborhoods of the *pseudo-minima* of Δ_T which are $O(T^{-1/2})$ perturbations of $\mathcal{C}_\ell$. In particular, for each j and each fixed $\varepsilon \in (0, r_j)$,

$$\mathbb{P}\Big(\widehat{C}_{T,f} \cap (c_j^\star - \varepsilon, c_j^\star + \varepsilon) \neq \emptyset\Big) \to 1, \qquad \mathbb{P}\Big(\widehat{C}_{T,f} \subset \mathcal{C}_\ell^\varepsilon\Big) \to 1.$$

The point ∞, if present in the implemented constraint set, is handled by the scalar selection rule defining $\widehat{C}_{T,\infty}$. Operationally, this means that using the same localized set in the full sample and all subsamples continues to target the correct finite set of pseudo-binding points, together with the relevant mean component when it is selected, and the induced tangent-cone geometry is unchanged up to $o_p(1)$ perturbations.

OIKONOMIKO ΠΑΝΕΠΙΣΤΗΜΙΟ ΑΘΗΝΩΝ ATHENS UNIVERSITY OF ECONOMICS AND BUSINESS ΣΧΟΛΗ ΟΙΚΟΝΟΜΙΚΩΝ ΕΠΙΣΤΗΜΩΝ SCHOOL OF ECONOMIC SCIENCES ΤΜΗΜΑ ΟΙΚΟΝΟΜΙΚΗΣ ΕΠΙΣΤΗΜΗΣ DEPARTMENT OF ECONOMICS

Department of Economics
Athens University of Economics and Business

List of Recent Working Papers

2024

01-24 Market Timing & Predictive Complexity, Stelios Arvanitis, Foteini Kyriazi, Dimitrios Thomakos
02-24 Multi-Objective Frequentistic Model Averaging with an Application to Economic Growth, Stelios Arvanitis, Mehmet Pinar, Thanasis Stengos, Nikolas Topaloglou
03-24 State dependent fiscal multipliers in a Small Open Economy, Xiaoshan Chen, Jilei Huang, Petros Varthalitis
04-24 Public debt consolidation: Aggregate and distributional implications in a small open economy of the Euro Area, Eleftherios-Theodoros Roumpanis
05-24 Intangible investment during the Global Financial Crisis in the EU, Vassiliki Dimakopoulou, Stelios Sakkas and Petros Varthalitis
06-24 Time will tell! Towards the construction of instantaneous indicators of different agent-types, Iordanis Kalaitzoglou, Stelios Arvanitis
07-24 Norm Constrained Empirical Portfolio Optimization with Stochastic Dominance: Robust Optimization Non-Asymptotics, Stelios Arvanitis
08-24 Asymptotics of a QLR-type test for optimal predictive ability, Stelios Arvanitis
09-24 Strongly Equitable General Equilibrium Allocations, Angelos Angelopoulos
10-24 The Greek macroeconomy: A note on the current situation and future outlook, Apostolis Philippopoulos
11-24 Evolution of Greek Tax System, A Survey of Legislated Tax Changes from 1974 to 2018, Panagiotis Asimakopoulos
12-24 Macroeconomic Impact of Tax Changes, The case of Greece from 1974 to 2018, Panagiotis Asimakopoulos
13-24 `Pareto, Edgeworth, Walras, Shapley' Equivalence in a Small Economy, Angelos Angelopoulos
14-24 Stimulating long-term growth and welfare in the U.S, James Malley and Apostolis Philippopoulos
15-24 Distributionally Conservative Stochastic Dominance via Subsampling, Stelios Arvanitis
16-24 Before and After the Political Transition of 1974. Institutions, Politics, and the Economy of Post-War Greece, George Alogoskoufis
17-24 Gaussian Stochastic Volatility, Misspecified Volatility Filters and Indirect Inference Estimation, Stelios Arvanitis, Antonis Demos
18-24 Endogenous Realtor Intermediation and Housing Market Liquidity, Miroslav Gabrovski, Ioannis Kospentaris, Victor Ortego-Marti
19-24 Universal Choice Spaces and Expected Utility: A Banach-type Functorial Fixed Point, Stelios Arvanitis, Pantelis Argyropoulos, Spyros Vassilakis

Πατησίων 76, 104 34 Αθήνα. Τηλ.: 210 8203303-5. E-mail: econ@aueb.gr / www.aueb.gr
76, Patission Street, Athens 104 34 Greece. Tel.: (+30) 210 8203303-5

2025

01-25 Democracy, redistribution, and economic growth: Some evidence from post-1974 Greece, George C. Bitros

02-25 Assessing Downside Public Debt Risks in an Environment of Negative Interest Rates Growth Differentials, Yiannis Dendramis, Georgios Dimitrakopoulos and Elias Tzavalis

03-25 Wicksellian General Equilibrium, Angelos Angelopoulos

04-25 Institutions and Ethics, Angelos Angelopoulos

05-25 General Equilibrium in a Capitalist Economy, Angelos Angelopoulos

06-25 Public investment multipliers revisited: The role of production complementarities, Vasiliki Dimakopoulou, George Economides, and Apostolis Philippopoulos

07-25 The heterogeneous causal effects of the EU's Cohesion Fund, Angelos Alexopoulos, Ilias Kostarakos, Christos Mylonakis, and Petros Varthalitis

08-25 Gaussian Invariant Markov Chain Monte Carlo, Michalis K. Titsias, Angelos Alexopoulos , Siran Liu, and Petros Dellaportas

09-25 Financial Intermediation, Investment, and Monetary Policy, Ioannis Kospentaris and Florian Madison

10-25 Temperature as a premium factor. Insurance incorporating climate change. A comparative case study between Europe and North America, Nomikou-Lazarou Irene

11-25 How High will our Buildings Become? Angelos Angelopoulos

12-25 Emergency Room General Equilibrium, Angelos Angelopoulos

13-25 Updating Density Estimates using Conditional Information Projection: Stock Index Returns and Stochastic Dominance Relations, Stelios Arvanitis, Richard McGee, and Thierry Post

14-25 Measuring Textual Cohesion via Graph Curvature, Weighted Dominance, and Embedding-Based Coherence, Stelios Arvanitis

15-25 Universal Preference Spaces for Expected Utility via a Banach-type Functorial Fixed Point, Stelios Arvanitis, Pantelis Argyropoulos, and Spyros Vassilakis

16-25 Planet Earth's General Equilibrium, Angelos Angelopoulos

17-25 Electable and Stable Insiders' Coalition Governments, Tryphon Kollintzas and Lambros Pechlivanos

18-25 Long Memory from Cheeger Bottlenecks and Long Cycles in Network Dynamics, Stelios Arvanitis

19-25 Robust Multiobjective Model Averaging in Predictive Regressions, Stelios Arvanitis, Mehmet Pinar, Thanasis Stengos, and Nikolas Topaloglou

20-25 On robust Bayesian causal inference, Angelos Alexopoulos and Nikolaos Demiris

21-25 Leverage Effect, Volatility Feedback and the Influence of Jumps, Orestis Agapitos, Ioannis Papantonis, Leonidas Rompolis, and Elias Tzavalis

22-25 Leadership: The other deficit of post-1974 Greece, George C. Bitros

2026

01-26 The Tell-Tale Clock! Speed and Agent Composition in High Frequency Trading, Stelios Arvanitis

02-26 Sentiment Utopia Index: Rhetorical Structure and Corpus-Relative Financial Sentiment, Stelios Arvanitis

03-26 Draghi's report a year later: Beneficial but no remedy for EU challenges, George C. Bitros, Anastasios G. Malliaris, and Mark S. Rzepczynski

04-26 **Tax Structure Reform and Macroeconomic Strategy in Greece: Econometric Evidence and Policy Implications, Panagiotis Asimakopoulos**

05-26 **A Perspective on International Monetary Leadership. From Silver and Gold to the Dollar Standard, George Alogoskoufis**

06-26 **Behavioral Balanced Scorecard Framework for Tax Administrations: Integrating Tax Morale, Institutional Trust, and Compliance Behavior, Panagiotis Asimakopoulos**

07-26 **Education and governance: The Russell–Hayek Conundrum through the lenses of ancient Sparta and the "Sparta of the East", George C. Bitros**

08-26 **Overhauling Democracy: Layered State Authority, Corporate-Style Accountability, and the Free Market Economy, George C. Bitros and Steve Bakalis**

09-26 **ECONOMICS 200. The Economics of transition to a Steady State Economy, Theodore P. Lianos**

10-26 **Empirical Likelihood Tests for Pairwise Stochastic Dominance, Stelios Arvanitis, Richard McGee, and Thierry Post**

Department of Economics
Athens University of Economics and Business

The Department is the oldest Department of Economics in Greece with a pioneering role in organising postgraduate studies in Economics since 1978. Its priority has always been to bring together highly qualified academics and top quality students. Faculty members specialize in a wide range of topics in economics, with teaching and research experience in world-class universities and publications in top academic journals.

The Department constantly strives to maintain its high level of research and teaching standards. It covers a wide range of economic studies in micro-and macroeconomic analysis, banking and finance, public and monetary economics, international and rural economics, labour economics, industrial organization and strategy, economics of the environment and natural resources, economic history and relevant quantitative tools of mathematics, statistics and econometrics.

Its undergraduate program attracts high quality students who, after successful completion of their studies, have excellent prospects for employment in the private and public sector, including areas such as business, banking, finance and advisory services. Also, graduates of the program have solid foundations in economics and related tools and are regularly admitted to top graduate programs internationally. Three specializations are offered:1. Economic Theory and Policy, 2. Business Economics and Finance and 3. International and European Economics. The postgraduate programs of the Department (M.Sc and Ph.D) are highly regarded and attract a large number of quality candidates every year.

For more information:

https://www.dept.aueb.gr/en/econ/

Πατησίων 76, 104 34 Αθήνα. Τηλ.: 210 8203303-5. E-mail: econ@aueb.gr / www.aueb.gr
76, Patission Street, Athens 104 34 Greece. Tel.: (+30) 210 8203303-5